Facultade de Ciencias

Grao en Química

Memoria do Traballo de Fin de Grao

A study of advanced oxidation processes for the degradation of emergent organic micropollutants

Estudio de procesos de oxidación avanzada para la degradación de microcontaminantes orgánicos emergentes

Estudo de procesos de oxidación avanzada para a degradación de microcontaminantes orgánicos emerxentes

Francisco Javier Ayala Esmoris
Curso: 2020 - 2021. Convocatoria: Xuño

Director: Moisés Canle López

A mi abuelo,

Index

Abstract / Resumo / Resumen

The Green Revolution and massive industrialization of agriculture led to an increase in the use of organic and inorganic pesticides, which threat both the environment and health of plants, animals and humans. In this respect, we have studied the potential application of advanced oxidation processes (UV photolysis, UV photocatalysis) as remediation technologies for elimination / reduction of the diffusse occurrence of persistent organic pollutants. Among these, we selected a neonicotinoid pesticide, imidacloprid (IMD) as one of the members of the EU Watch List of emerging water pollutants, and the obtained results will be discussed. Different variables that are relevant for the process have been studied, such as pH, concentration of IMD and photocatalyst, composition of the atmosphere (% O_2), and temperature will be taken into consideration.

The adsorption process, the photolysis process and their kinetics, efficiency and photoproducts have been studied, and a proposal was made for reaction pathways leading to the different photoproducts.

Keywords: Neonicotinoids, Imidacloprid, Photochemistry, Heterogeneous Photocatalysis, AOPs, Wastewater, POPs

A Revolución Verde e a masiva industrialización da agricultura levou a un aumento no emprego de pesticidas orgánicos e inorgánicos, os cales ameazan ao medio ambiente e a saúde das prantas, animais e humanos. Respecto a isto, estudiamos a potencial aplicación de procesos de oxidación avanzada (fotólisis UV, fotocatálisis UV) coma tecnoloxías de remediación ou eliminación / redución da incidencia difusa de contaminantes orgánicos persistentes. Entre estes, seleccionamos un pesticida neonicotinoide, o imidacloprid (IMD) como un dos membros da Lista de Vixianza da UE de contaminantes emerxentes en auga, e os resultados obtidos serán discutidos. Diferentes variables relevantes para o proceso foron estudiados, coma o pH, a concentración de IMD e fotocatalizador, a composición da atmosfera (% O_2), e a temperatura serán tomadas en consideración.

O proceso de adsorción, o proceso de fotólise e as súas cinéticas, a eficiencia e os fotoprodutos foro estudiados, e unha ruta de reacción que conduce aos diferentes fotoprodutos foi proposta.

Palabras chave: Neonicotinoides, Imidacloprid, Fotoquímica, Fotocatálise Heteroxénea, AOPs, Augas residuais, POPs

La Revolución Verde y la masiva industrialización de la agricultura llevaron a un aumento en el empleo de pesticidas orgánicos e inorgánicos, los cuales amenazan al medio ambiente y la salud de las plantas, animales y humanos. Respecto a esto, estudiamos la potencial aplicación de procesos de oxidación avanzada (fotólisis UV, fotocatálisis UV) como tecnologías de remediación o eliminación / reducción de la incidencia difusa de contaminantes orgánicos persistentes. Entre estos, seleccionamos un pesticida neonicotinoide, el imidacloprid (IMD) como uno de los miembros de la Lista de Vigilancia de la UE de contaminantes emergentes en el agua, y los resultados obtenidos serán discutidos. Diferentes variables relevantes para el proceso fueron estudiadas, como el pH, la concentración de IMD y fotocatalizador, la composición de la atmósfera (% O_2), y la temperatura serán tomadas en consideración.

El proceso de adsorción, el proceso de fotólisis y sus cinéticas, la eficiencia y los productos fueron estudiados, y una ruta de reacción que conduce a los diferentes fotoproductos fue propuesta.

Palabras clave: Neonicotinoides, Imidacloprid, Fotoquímica, Fotocatálisis Heterogénea, AOPs, Aguas residuales, POPs

Introduction

The Green Revolution, sometimes called Third Agricultural Revolution, led to the diversification of new technologies. These technologies were focused on the research of new varieties of cereals, synthetic fertilizers, and intelligent irrigation, among others, with the aim to increase agricultural production worldwide. However, even when bringing advancements on many scientific fields and solving famine and malnutrition in many places around the world, it also brought several inconveniences: reduced agricultural biodiversity, increased the dependency on fossil fuels for machinery, transport, pesticides production, and introduced health effects of pesticides on both humans and wildlife, mostly amphibians and insects.

On the latter, there are evidence that link the application of pesticides with the so-called Colony Collapse Disorder (CCD) **[1]**, in which many or all the working bees abandon the colony, leaving behind the queen bee. This phenomenon has been reported many times in the past but has increased in the last 20-30 years. It is known that most of pollinators, among which we can find honeybees, contribute to an estimated 22 billion euros each year to the European agriculture industry. These insects are essential for the pollination of roughly 80% of crops and wild plants in our continent **[2]**. In January 2013, the EFSA (*European Food Safety Authority*) started to monitor the potential harmful effects of several neonicotinoids (thiamethoxam, imidacloprid and clothianidin) on bees' well-being, which ended stating in February 2018 the need of restrictions on the use of these pesticides because of the threat they pose on bees' health. Such is the risk that on April 27th, 2018, the EU decided to ban the use of these three neonicotinoids in open fields, restricting their use exclusively to closed greenhouses **[3]**.

Thus, this work will focus on these compounds, the neonicotinoids (displayed in *Figure 1*) and more precisely, on imidacloprid. Neonicotinoids are compounds derived from nicotine which have been widely commercialized and used as pesticides since the early 1990s **[4]**. These compounds affect the cholinergic system of insects, found in the central nervous system (CNS), whereas in mammals and other vertebrates it is located in the peripheral and central nervous system. Thus, for its use as an insecticide, this compound has to travel into the CNS, where it will bind irreversibly to the nicotinic acetylcholine receptor, also known as nAChR, straight at the synapse. This will affect neural functions and kill the insects by inducing paralysis **[5]**.
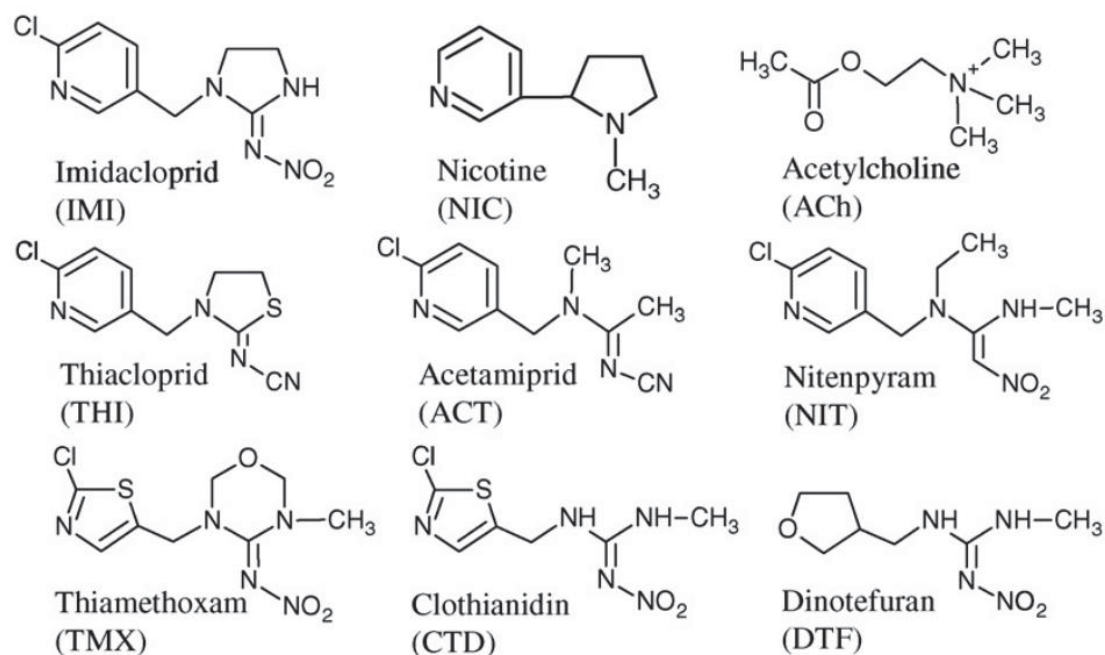
Figure 1.- *Chemical structure and abbreviatures of nicotine and some of its main nicotinoid derivatives*

Imidacloprid is used for reducing several pests, like sucking insects, soil insects, termites, etc. It is mainly applied to the surface of seeds, although it is also used on crops. It has a very low vapor pressure (1×10^{-7} mmHg), making this compound not readily volatile. Therefore, it is not easily dispersed by air. Its photolysis half-life at the soil surface can range from 27 to 229 days. Also, its high-water solubility (514 mg/L at 20° C and pH 7) facilitates imidacloprid leaching to ground water [6]. Furthermore, this compound, and many other pesticides, can lixiviate into subterranean water sources, bioaccumulate in plants or animals, and even harm or eliminate non-target insects. These are the reasons why imidacloprid is being studied as a potential *persistent organic pollutant* (POP) and why it was included in the EU Watch List of emerging pollutants in aquatic environments in 2015 [7].

As this compound is seen as a potential health threat, not only to insects and small vertebrate's well-being, but also to humans, there is a need to investigate its efficient degradation. Thus, the focus should be centered around wastewater treatment stations and how to "update" them in order to decrease the concentration of many POPs in solution, since they are nowadays successful on eliminating many toxic substances from drinkable water, but they are not powerful enough to degrade persistent pollutants. One of the most widely investigated and effective methods to degrade these compounds are *Advanced Oxidation Processes* (AOPs). These are processes that use hydroxyl radicals

(HO˙), the most reactive oxidizing agent applied in water treatment and wastewater for destruction of organic and/or inorganic contaminants.

Therefore, this work will focus on the degradation of imidacloprid by AOPs. Among the many AOPs, photochemical and chemical processes from both homogeneous and heterogenous phase AOPs will be taken in consideration.

Some examples of homogeneous AOPs are:
- UV photolysis
- Photo-Fenton
- UV/O_3
- UV/H_2O_2
- O_3/H_2O_2
- Ultrasound
- $Ultrasound/H_2O_2$
- $Ultrasound/O_3$

Some types of heterogenous AOPs are:
- $UV/O_3/TiO_2$
- $UV/H_2O_2/TiO_2$
- $UV/H_2O_2/catalyst$
- Catalytic ozonation
- $H_2O_2/catalyst$

Both methods studied in this work be based mainly on UV photolysis and UV/TiO_2 systems and other photocatalysts. These methods will be introduced and explained on their physico-chemical basis. Prior to the photocatalytic study, adsorption onto the photocatalytic surface is needed, and therefore has to be investigated under different experimental conditions. The kinetics of degradation of IMD in relation to both methods will be presented. The degradation photoproducts of IMD at different times of irradiation will be characterized, and their toxicity will be studied deeply with microalgae cultures (not a subject of this work, but of a parallel one for the Degree in Biology).

Objectives

The objective of this essay is to carry out several AOP experiments on imidacloprid and try to infer which method is the optimum to degrade this pesticide from drinkable and mainly agriculture-purpose water. These experiments will be carried out under different conditions, such as temperature, pH, concentration of imidacloprid and radiation.

The main goal of this dissertation is to study a suitable and effective AOP for IMD remediation in solution. For that, the degradation of IMD, the time required for the process and the influence of different conditions such as the pH, the initial concentration of the reagents or atmosphere composition will be considered.

Further, AOP products will be identified. Given that these are photolytic processes, and that a variety of products may be generated, only those with relevant concentration will be considered for further study.

Background

Water of good quality is essential for agriculture, irrigation and overall, the well-being of our environment and our health. However, the different sources of drinking water are constantly subject to pollution and contamination, and therefore require a correct treatment in order to eliminate and/or remove harmful contaminants. Among various sources of contamination, the most common are naturally occurring chemicals, that are strongly conditioned by local land practices and agriculture (such as the use of fertilizers, pesticides, etc) [8]. Chemicals of recent or new use, like fertilizers, pesticides, household products or pharmaceutical drugs are usually known as *emerging contaminants* (EC), since they pose a risk to our health, animals' health and a threat to the environment that is not fully understood [9].

As a consequence, the presence of pollutants and harmful compounds in water can derive into adverse effects to our health, such as gastrointestinal diseases, fertility issues, and neurological illnesses.

These chemicals are not completely degraded after application, meaning that many metabolites and even part of non-metabolized compounds are excreted and subsequently enter the ecosystem [10]. However, this does not mean a threat when

these metabolites have a very short half-life in solution and/or soil by the action of solar irradiation, oxidation or hydrolysis, and when their degradation products are not harmful (or at least not as much) as the original compound. When these metabolites are inert to the medium, have a very long half-life and/or imply a threat to the well-being of the environment, they are called *Persistent Organic Pollutants* (POPs).

Since drinking water is constantly exposed to pollution, there is a need for appropriate and effective treatment methods to remove harmful agents. Wastewater systems apply different treatment methods to prepare clean and safe water for disposal into nature. Water treatment processes include coagulation and flocculation (precipitation of dirt and other dissolved particles), sedimentation (settling of particles due to their weight), filtration (selective removal of dissolved particles due to their size), and disinfection (addition of disinfectants, such as chlorine, or use of other oxidation technologies), in order to eliminate harmful microorganisms [11]. Many of the steps involved in water treatment rely on transfer of the pollutant among different media, rather than on degrading / destroying it. Furthermore, POPs are usually very difficult to eliminate since their concentration in water is usually at ppm or ppb. Thus, the need for processes able to transform these harmful POPs into non-toxic products, that can be applied on dilute waste streams.

Among the most promising alternative treatment processes for the removal of POPs are *Advanced Oxidative Processes* (AOPs) [12]. These processes were first proposed for their use in drinking water treatment in the 1980s and later were investigated for their application on wastewater. They are based on the use of powerful hydroxyl radicals as a major oxidizing agent. These highly oxidizing agents can easily degrade recalcitrant organic pollutants (like POPs) and eliminate inorganic contaminants in wastewater. AOPs are mostly applied for the destruction of POPs and their transformation into less or non-harmful metabolites/products [13].

Few years after the term AOPs was coined by Glaze in 1987, Peyton et al presented to the Waste Management and Research Center of Illinois in 1989 a *"mobile oxidation pilot plant (MOPP)"*, in order to build a skid or transportable pilot plant that could cleanup of pollution water sources in remote locations. To test the pilot plant, they underwent several experiments of degradation to trichloroethylene (TCE), a common ground-water contaminant. The methods applied were bubbling with oxygen, ozonation, and ozone/UV degradation. The fastest and most effective method was ozone/UV oxidation, which had a rate of degradation 20% greater than simple ozonation. As the possible future uses of

the *MOPP*, they concluded that the pilot could be applied for the removal of organic pollutants in industrial wastewater and ground water. Among the most relevant contaminants considered, we can highlight chlorinated ethenes, PAHs, phenols and most importantly, pesticides [14].

AOPs had diversified ever since 1987, many times including methods in which UV is accompanied by oxidizing compounds, like ozone, H_2O_2, and sometimes also been helped by photocatalysts. The latter usually are semiconductor materials, such as TiO_2, that show great potential in AOPs, since they have greater photochemical stability. They also decrease the activation energy and increase the rate of reaction, while having high surface are, low cost and non-toxicity. Agüera et al. were some of the first researchers to study the degradation of IMD, one of the most problematic (and most restricted) pesticide nowadays, through photocatalysis supported with TiO_2 in 1998. They concluded that, after 450 min of oxidation, the presence of both IMD and its degradation products (such as chloronicotinic acid and chloronicotinic aldehyde) was practically negligible in solution [15].

Under UV-Vis light, an e^- from a bonding or non-bonding MO from a POP is promoted into an antibonding MO, according to "vertical" transitions defined by the Frank-Condon principle. Given that this process can undergo spin inversion or not, the excited species may end up with two unpaired electrons with parallel or anti-parallel spins. Those with anti-parallel spins are singlet states, ^1POP, while those with parallel spins are triplet states, ^3POP. The reactivity of these two possible states is usually very different: singlets, defined as "closed-shell" species, usually react with other closed-shell compounds, while triplets, being open-shell, may react with any other open-shell species ('quantum kinetic impediment').

However, many POPs absorb almost no Vis light. These substances are designed not to undergo structural changes, and Vis light absorption can induce them, implying loss in their chemical properties. An alternative would be the use of UV light, much more energetic that Vis light, and hence more effective for the degradation of POPs. Nevertheless, UV light is also more expensive and harmful to living beings.

In order to avoid the inconveniences of UV light, many alternatives, such as photo-Fenton or photosensitized processes, have been proposed. Among these proposals, photocatalysis is one of the most widely used and studied alternatives nowadays. This process is based on the use of a semiconductor with an energy gap (E_G) appropriate to

be overcome by Vis light, fulfilling the resonance condition ($\Delta E = h \cdot \nu$). Upon sunlight absorption, an electron is promoted from the valence band into the conduction band, leaving a positive vacancy (a 'hole', h^+) in the valence band, and as a consequence, an electron-hole pair (h^+- e^-) is formed.

Most of the h^+ - e^- pairs are annihilated in pico- or nanoseconds, liberating energy in the process. Some of these h^+ - e^- pairs live long enough to migrate to the surface of the photocatalyst and react with any substance that may adsorbed. In this process, water molecules or even hydroxyl groups adsorbed onto the surface undergo oxidation by h^+, yielding $HO^\cdot$ radicals. On the other side, O_2 molecules adsorbed to the surface undergo reduction by e^-, yielding $O_2^{\cdot-}$ radicals. These radicals can undergo protonation and yield their conjugated acid, $HO_2^\cdot$. The whole set of processes take place on the surface, and not in the bulk of the solution, so surface chemistry is a vital part of any heterogeneous catalysis process.

$HO^\cdot$ and h^+ are major oxidizing agents, with $E^0(HO^\bullet/HO^-)=2.27$ V vs. NHE, $E^0(h^+)=2{,}53$ V vs. SHE, and may degrade any substance present in solution, such as POPs. Given that these processes involve the use of radicals, many photoproducts are expected. Further, the constant production of these oxidizing agents implies the degradation of primary products, secondary products, etc. Hence, complete mineralization is sometimes achieved in photocatalysis. *Figure 2* displays the reactions and processes involved in a photocatalysis reaction.
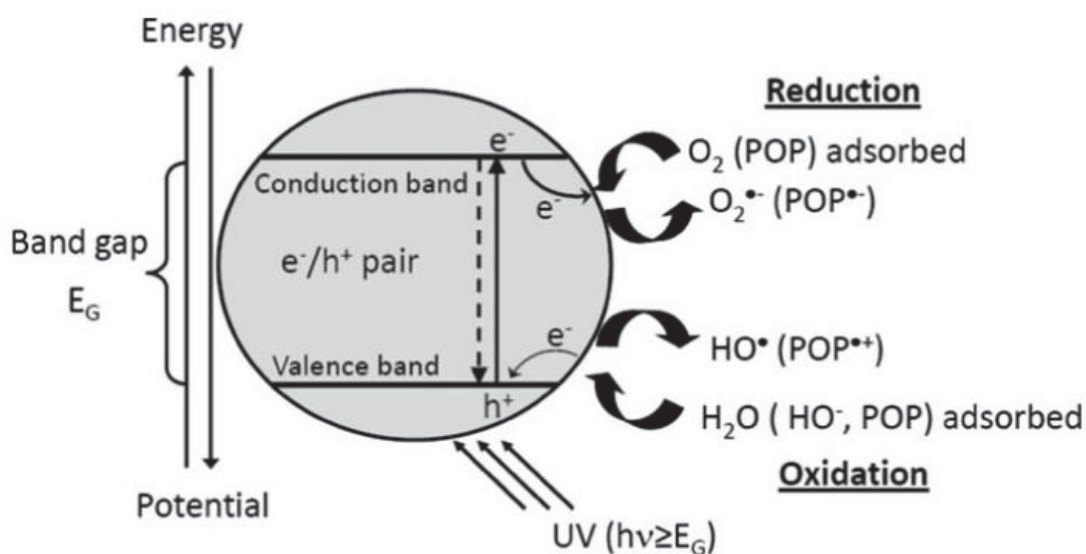

Figure 2.- *Diagram of the reactions involved in a photocatalysis process in a semiconductor surface [16]*

Materials and Methods

To study the influence of pH on the UV/Vis spectra, 10 mL solutions of IMD at increasing concentrations (starting from 1 ppm up to 25 ppm) were prepared from a stock solution of 25 mL of IMD 200 ppm. Samples of different concentrations of imidacloprid (IMD) were measured at different pHs. For this, the pH was adjusted using HCl and NaOH. A JASCO V-560 UV-Vis spectrophotometer was used to measure the spectra.

To study the adsorption process, flasks of 10 mL were filled with solutions of 5-10 ppm of IMD using an increasing concentration/mass of catalyst. These were left under stirring in the dark, in a water bath at 25º C, and clean samples were taken at equally spaced times. The UV/Vis spectra of each sample were recorded. The samples were placed back to the flask after measurement.

The potential lixiviation of Cu^{+2} from the TiO_2/Cu was tested. For this, about 0,02 g of TiO_2/Cu were diluted in distilled water in 4 beakers. Prior to this, the mass of each beaker was recorded for later calculations. Afterwards, 2 beakers were left under stirring for about 24 h, while the other 2 were left for 48 h. After this time, the solutions were filtered with a syringe through a 0,45 μm pore glass fiber filter. The mass of the remaining solid was determined by mass difference with the beaker.

In the photolysis experiments, 250 mL solutions of IMD were placed in an UV reactor. The solution was irradiated with 254 nm UV light and samples were taken at equally spaced times. For photocatalysis, a specific mass of catalyst was added into the solution. All reactions were carried out at 298.0 K under controlled atmosphere, in terms of % O_2. The UV/Vis absorbance of the samples was monitored to test the degradation of IMD. The irradiation source was a Heraeus TQ 150 medium-pressure Hg-vapor lamp, with intense emission lines at excitation = 254, 313, 366, 405, 436, 546 and 578 nm, located axially in the reactor inside a quartz immersion tube. The UV lines at excitation < 366 nm were filtered out using a DURAN 50® glass jacket filled with water, limiting the irradiation to near UV–visible (NUV–Vis).

Photocatalytic degradation of IMD under sunlight was studied using 250 mL solution of IMD 5 ppm, kept under the sun for 3 h in transparent bowls, covered with transparent lids to avoid evaporation. A thin layer of BP50/P25 pellets was placed in the bottom of the bowls. A sheet of aluminum foil was placed under the bowls in order to maximize the reflection of sunlight. A similar bowl containing the same amount of pellets with distilled

water was also treated in the same conditions. Samples were taken from the solutions at regularly spaced times. The UV-Vis spectrum of each sample was measured in order to determine the expected degradation of IMD.

HPLC-DAD (Thermo Fisher LC instrument, equipped with a multi-channel pump and a L-2450 diode array detector) and HPLC-MS (Agilent 1290 Infinity II apparatus, coupled with Agilent 6546LC/QTOF) were used to characterize the photodegradation products. The HPLC-DAD experiments were made with a RESTEK LC C-18 column (250 x 4,6 mm, 5 μm) column, operated at room temperature with elution solvents A (Milli-Q water) and B (acetonitrile) at flow rate of 1 mL·min^{-1}. The isocratic mobile phase was of 40:60 A:B. The volumes injected were 50 μL. A Hypersyl Gold C4 column (150 × 2.1 mm, 3μm) was used, operated at 25°C with elution solvents A (0.1% formic acid) and B (0.1% methanol) at flow rate of 250 μL·min^{-1}. The gradient was as follows: 0-1 min, 80-80% A and 20-20% B; 1-5 min, 80-0% A and 20-100% B; 5-10 min, 0-0% A and 100-100% B; 10-11 min, 0-80% A and 100-20% B; 11-14 min, 80-80% A and 20-20% B. Injection volume was 20 μL. For the HPLC-MS experiments, positive ion mode electrospray (ESI+) was used, with 210 ºC gas temp., drying gas circulating at 13 L/min, nebulizer set at 35 psi, sheath gas temp. set at 350 ºC, sheath gas flow at 11 L/min, vCap at 4000 V and an applied potential of 130 V on the fragmentor. The analyses were carried out using full-scan data dependent MS scanning from m/z 50 to 500.

Working plan and Schedule

The working plan and schedule of this end-of-degree dissertation have been slightly affected by the restrictions linked to the COVID-19 pandemic.

During October, the tutors of both Chemistry and Biology end-of-degree projects and the student discussed a first rough draft of organization of the working plan. They decided that the student should focus mainly on the Chemistry project during at least the first semester of the school year, while he would leave the elaboration of the Biology project for the remaining time of the year.

During the last week of that month the student focused on gathering information about the pesticide (chemical and structural properties, safety, legislation focused on its application, etc).

In November, the main experiments carried out were influence of pH on absorbance and adsorption to surface experiments. However, at mid-November, the experiments had to be delayed due to the student having caught COVID-19. The experiments were resumed mid-December.

The photolysis, determination of degradation constant, and characterization of degradation products experiments were carried out from January until May. However, photocatalysis experiments under sun light were carried out in June. The second semester was mostly devoted to refining some experiments and writing the final and definitive draft of this end-of-degree dissertation.

Results & Discussion

UV spectra of IMD at different pH

The experimental procedure was described previously in the Materials and Methods section. **Figure 3** shows the obtained results.
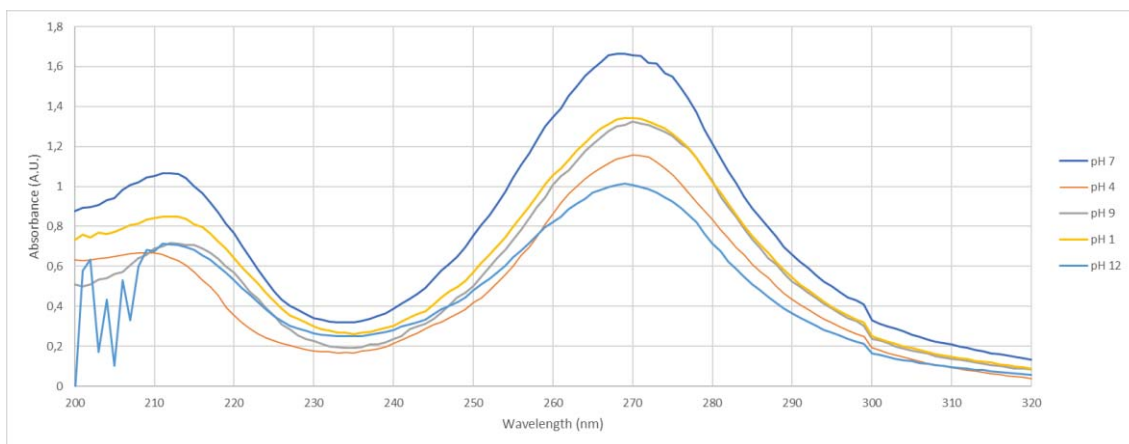
Figure 3.- *Spectra of IMD at different pH values. [IMD] = 15 ppm, room T*

Two maxima of absorbance at different pH values for IMD are seen in **Figure 3.** A maximum is observed at *ca.* 270 nm at all pH values, and a second less intense band at ca. 214 nm, also at all pH values. The corresponding molar absorptivity coefficient obtained from the Beer Law is ε(270 nm, pH=7) = 26671$\pm$1304 M$^{-1}\cdot$cm^{-1}, and does not vary with pH, with an average value ε(270 nm) = 22046$\pm$2646 M$^{-1}\cdot$cm^{-1}. This indicates the associated electronic transition is not affected by the state of protonation. Thus, changes in the concentration of IMD can be monitored by spectrophotometry.

Following the study of Wang et al., the absorption spectrum maximum at 270 nm is generated by the electronic transition between valence electron and electron in molecular orbital, which belonged to n $\rightarrow$ π^* transition, from nonbonding atomic orbital to molecular antibonding orbital with high level [17]. The molar absorptivity coefficient calculated is not compatible with such transition since it points to a $\pi \rightarrow \pi^*$ transition. To clarify this, solvatochromism studies would be necessary. The maximum at 214 nm is compatible with a $\sigma \rightarrow \sigma^*$ transition of electrons.

The presence of two maxima of absorption for IMD can be interpreted in two different manners: either IMD has two chromophores, responsible for the 214 and 270 nm maxima, or IMD has only one chromophore and another species found in solution is responsible for the other maximum of absorbance. It is known that water has a wide band of UV absorbance at 166,5 nm (n $\rightarrow$ σ^* transition), which results in the photodissociation of water into H^+ and OH^- [18]. Therefore, this 214 nm absorbance maximum will be monitored through the different experiments in order to infer whether IMD has two chromophores or an interaction of different nature in solution with water is responsible for this maximum.

As mentioned, no clear dependence is observed between absorbance and pH. The absence of shifts in wavelength maxima and the lack of appearance of new maxima in this pH interval imply that the chromophores involved in the UV/Vis spectrum of IMD are the same, and therefore, that the electron transitions that originate these maxima are also the same. Hence, their change in absorbance can be explained by changes of pH, and thus, by alterations on the ionization of the chromophores involved in the absorbance.

The observed phenomenon can also be interpreted through the different ionization states of IMD. IMD shows two pK_a values one at 1,56 and another one at 11,12. These pK_a values can be explained by comparison with analogue compounds. 2-chloropyridine has a $pK_a=0,49$ and a structure that matches the pyridine moiety of IMD. Hence, we can assume that N^I on the pyridine ring is responsible for the first pK_a of IMD. It is more troublesome to find analogues for the second pK_a of IMD since several N can be responsible of the ionization. Trimethylamine shows a $pK_a=9,80$, and a similar structure is observed around N^{II} on IMD while dimethylamine shows a $pK_a=10.73$. N^{III} on IMD resembles dimethylamine, for which we can assume a similar pK_a value of IMD. N^{IV} is an iminic structure, and the pKa of the conjugate acid of imines is usually around 5. Though

N^{IV} shows a strong inductive effect due to the presence of a $-NO_2$ group, such a strong change would not be expected. *Figure 4* depicts the different associations of N atoms forementioned.
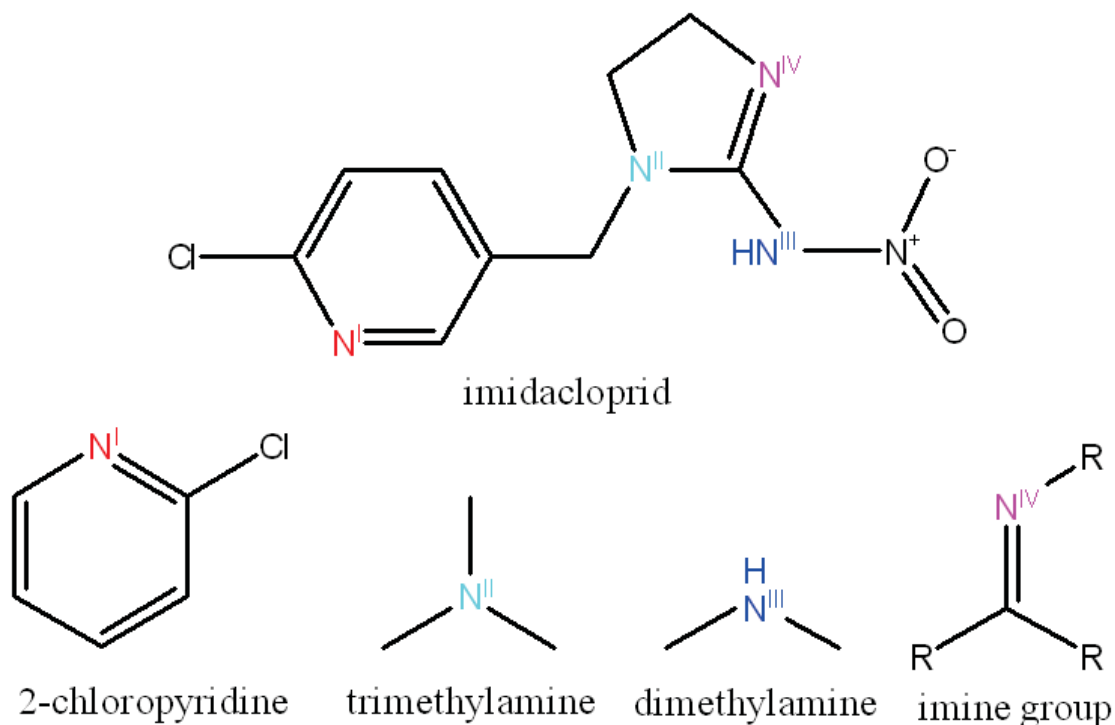

Figure 4.- *Association of the different N atoms on IMD to 2-chloropydinge, trimethylamine, dimethylamine, and imine group due to structural and chemical resemblance*

Through ionization of these functional groups, IMD is expected to have an overall positive charge at pH values lower than 1,56, while at pH values greater than 11,12, its charge should be negative. At intermedium pH values, IMD should be in a *zwitterionic* state, at which the overall charge should be neutral, due to the countereffect between positive and negative charges.

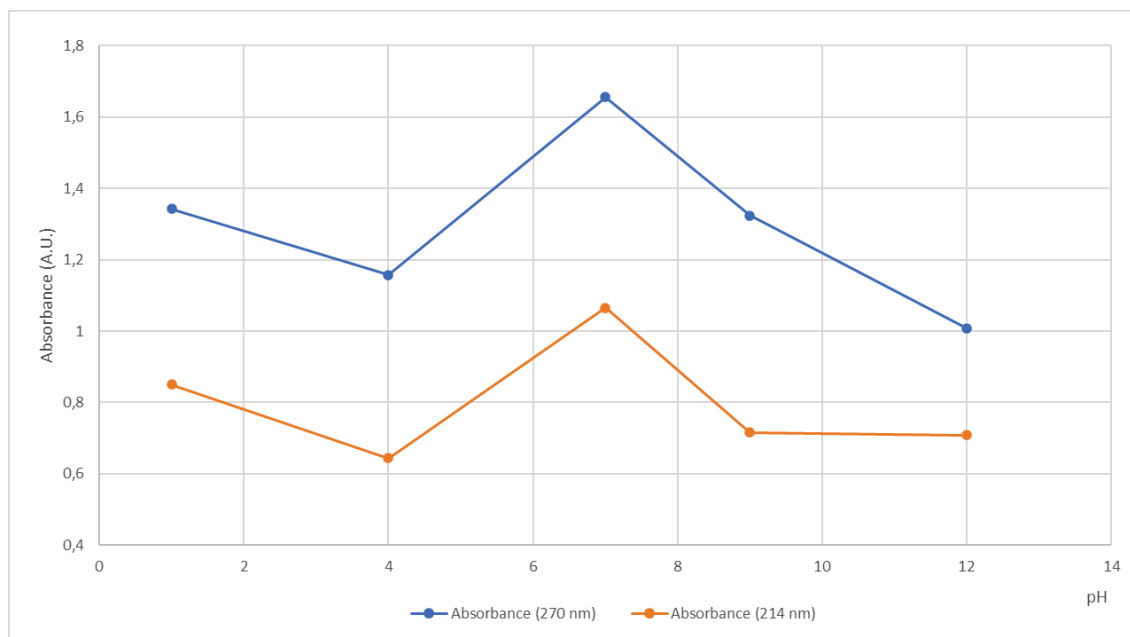*Figure 5* depicts the change in absorbance of both maxima (270 and 214 nm) for IMD with the variation of pH.

Figure 5.- *Absorbance of IMD at λ=270nm and λ=214nm at different pH values; [IMD] = 15ppm, room T*

Both maxima follow the same trend: their absorbance decreases from pH 1 to 4, goes through a maximum at pH 7, and then decreases for pH>9. The different ionization species of IMD have different molar absorptivities and hence the dependence of Abs *vs.* pH follows the pK_a distribution of the molecule. At neutral pH, where we should expect IMD to be in a *zwitterion* state, the absorbance of both maxima reaches their greatest value. Furthermore, we can conclude that the electronic transitions involved on both maxima are greatly favored by a *zwitterionic* state in IMD. The observed phenomenon can be interpreted through the electronic transitions responsible for both maxima. The lone electron pairs that undergo protonation usually correspond to antibonding molecular orbital electrons, and both electronic transitions involve this kind of molecular orbitals.

The bibliographic maximum of IMD is 270 nm; however, we can see an increase in absorbance at around 214 nm. This could mean two things: that IMD has two chromophores, responsible for the 214 and 270 nm maxima, or that IMD has only one chromophore and another species found in the solution is also responsible for the other maximum of absorbance. We know that water has a wide band of UV absorbance at 166,5 nm (n $\rightarrow$ σ* transition), which results in the photodissociation of water into H^+ and OH^- [18]. Accordingly, this 214 nm band undergo hipsochromic or bathochromic shifts, and also changes in intensity, depending on the acidity of the medium. Therefore, this 214 nm absorbance maximum will be monitored through the different experiments in order to infer whether IMD has two chromophores or if, in turn, changes in the composition of the medium are responsible for this maximum.

Adsorption study of IMD on different photocatalysts

Adsorption is the physicochemical process in which a molecule (called *adsorbate*; IMD in this study) interacts to a specific surface (stated as *adsorbent*). The process can be divided in two main events: *physisorption* and *chemisorption*. In *physisorption* processes, weak interactions are established between adsorbate and adsorbent, mainly associated to Van der Waals forces. In *chemisorption*, the interactions are stronger, involving electron exchange between the adsorbate and the adsorbent. This kind of bonding behaves as conventional covalent bonding.

Hence, the main difference between physisorption and chemisorption are the strength of the bonding interactions and the time in which each interaction takes place. The first one involves weak interactions; consequently, a quick adsorption followed by a fast desorption is expected by this kind of interaction. The second one involves very strong interactions, so a slow adsorption followed by no desorption is expected in this case.

In the experiments carried out, adsorption has been related to changes in the absorbance of IMD. Thus, a decrease in absorbance of IMD compared to its initial value would be related to the adsorption of the pesticide onto the catalyst. The opposite process would be related to its desorption.

Consequently, chemisorption would be evidenced by a slow steady decrease on IMD absorption and no or little desorption. Physisorption would be observed as a quick decrease on IMD absorbance followed by quick desorption. Physisorption is also linked to the reorganization of electron density in both adsorbate and adsorbent, and therefore, the net charge of each component at the moment of adsorption. It can be assumed that IMD is able to adsorb to the catalysts depending on its own and the catalysts' net charge. The net charge of both IMD and the catalyst at specific pH values can be predicted knowing their relative pK_a values and, consequently, physisorption can be expected.

The pK_a values of IMD are 1,56 and 11,12. Hence, at pH values lower than 1,56, IMD is expected to have a net positive charge. At intermedium pH values between 1,56 and 11,12, IMD is expected to have a net neutral charge, since it will behave as a *zwitterion*. At pH values higher than 11,12, IMD should have a net negative charge. In the case of SBA-15, it has a pK_a of 4,8. Therefore, at pH values higher than its pK_a, SBA-15 should have a net negative charge. TiO_2/Cu has a pK_a of 6,5, meaning that at pH values higher than that, this catalyst is expected to have a negative net charge. Given the composition

of BP50/P25 **[19]**, its surface will be easily protonated. Therefore, the interaction between IMD and the different surfaces studied is expected to be weak, in agreement with the hypothesis of physisorption.

The adsorption experiment for SBA-15 was carried out at pH 7. Hence, IMD is expected to have a neutral charge, while SBA-15 is expected to have a negative charge. Assuming these 2 conditions, a small adsorption of IMD onto SBA-15 could be expected. Something similar happens with TiO_2/Cu, where the experiments were carried out at pH 7,66. IMD is expected to behave as a *zwitterion* and TiO_2/Cu to have a negative charge; thus, some adsorption of IMD onto TiO_2/Cu should be observed, too.

For the adsorption experiments, the change in absorbance of IMD at different times was monitored, and the spectra obtained were overlapped to monitor changes. Furthermore, to infer the possible adsorption-desorption processes, the variation of absorbance at the different times was followed at both 270 nm and 214 nm.

- **SBA-15**

The experimental procedure was described previously in the Materials and Methods section. The measurements were carried out at regularly spaced times during 24 h, as indicated in **Figure 6**. The same kind of behavior was observed when using different loads of catalyst.
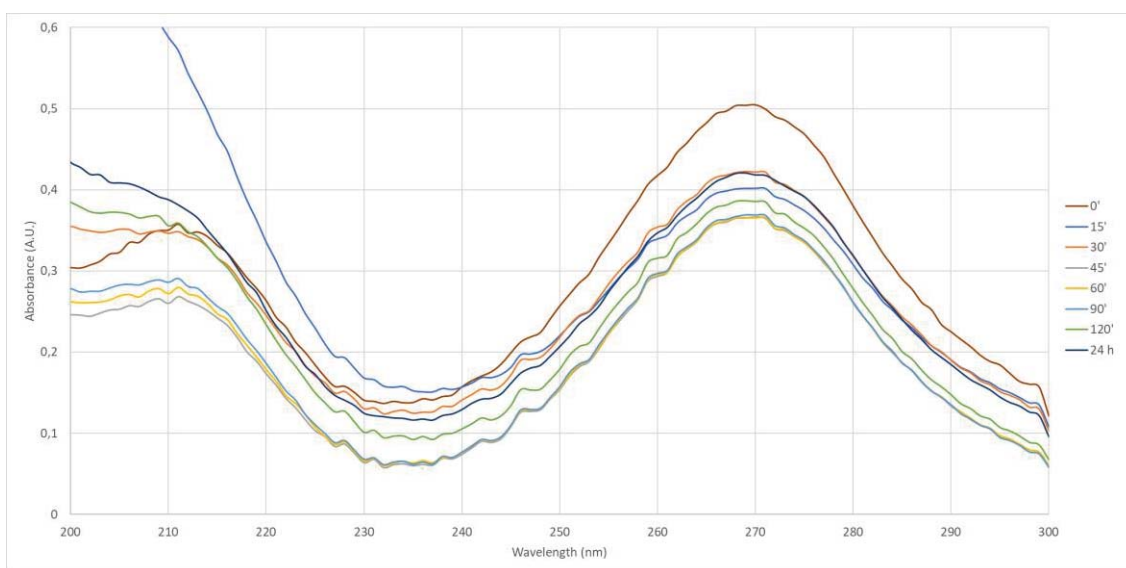

Figure 6.- *Time-resolved spectra of IMD adsorption over SBA-15. [IMD] = 5 ppm, [SBA-15] = 200 ppm, pH=7, 25ºC*

The variation of absorbance with time was monitored at λ = 270 nm, 214 nm to study the kinetics of adsorption, as depicted in **Figure 7** Thus, the study of the change of absorbance of IMD allow to monitor adsorption onto the surface of the catalyst. Th fact that absorbance decreases indicate IMD is adsorbing to SBA-15.
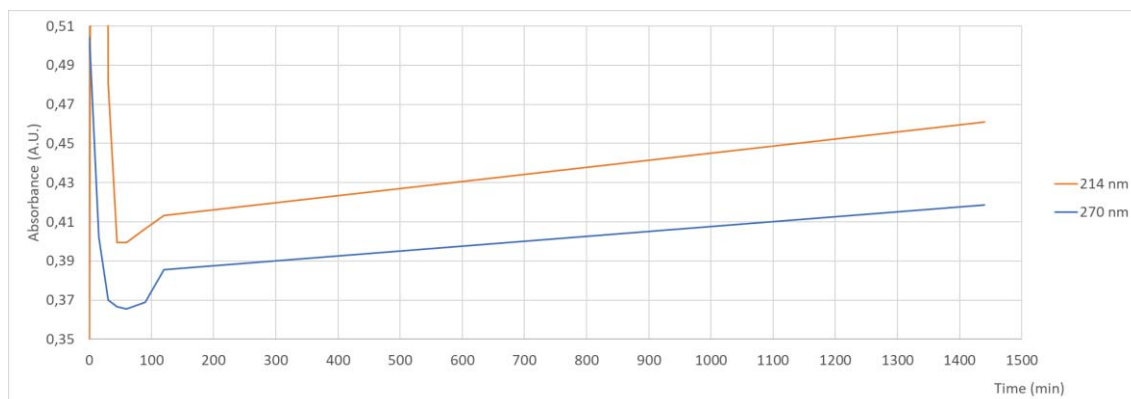

Figure 7.- *Evolution of absorbance of IMD at maxima λ=270nm and λ=214nm. [IMD]=5ppm, [SBA-15]=200ppm, pH=7, 25ºC*

A clear decrease of absorbance is observed during the first 90 min for both wavelengths, as shown in **Figure 7**, starting from 0,50 A.U. and dropping to 0,36 A.U. Then, the absorbance increases slowly until 0,41 A.U. after 24 h. A parallel behavior is observed at 214 nm from 15 min. The fast increase of absorbance during the first 15 min can be interpreted based on changes on the medium, as explained previously (see above).

Following the behavior at 270 nm, some adsorption takes place during the first 90 min (a decrease of 0,14 A.U.) This experiment was carried out at pH=7,47. From the corresponding Beer dependence (**Figure 8**) the concentration of IMD being adsorbed onto SBA-15 can be estimated:
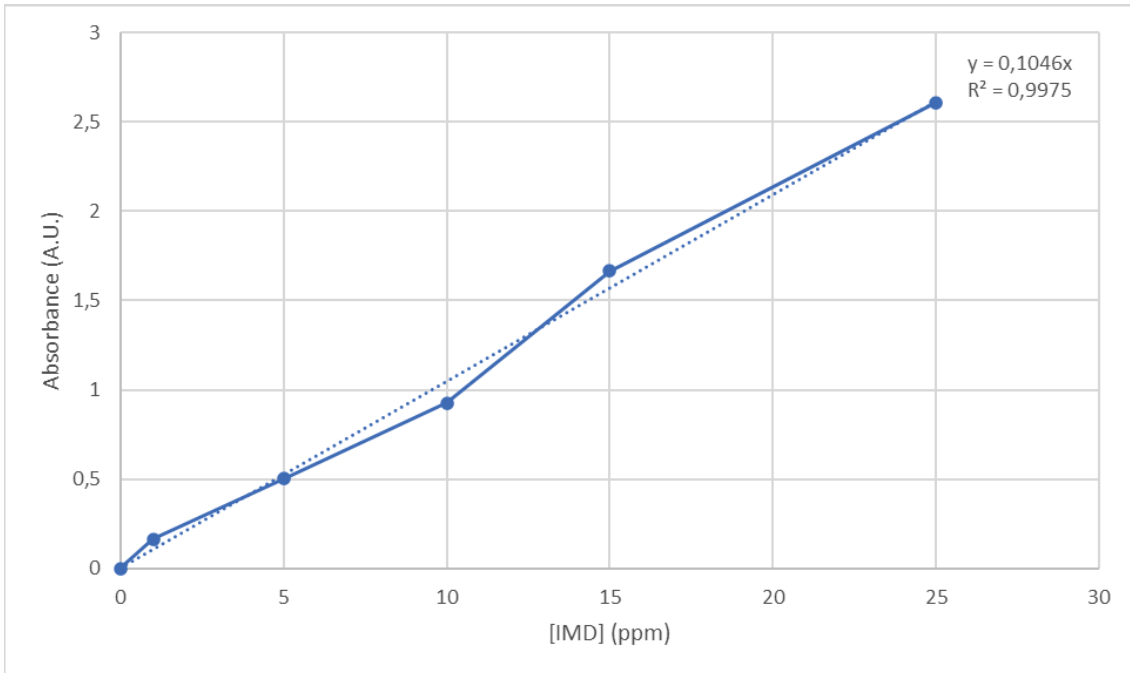
Figure 8.- *Calibration curve of IMD at pH=7. Concentration range: 1-25 ppm, 25ºC. Fitting equation disclosed in figure.*

$$\Delta Abs = 0{,}1046[IMD](ppm)$$

$$0{,}14 = 0{,}1046[IMD](ppm)$$

$$[IMD] = \frac{0{,}14}{0{,}1046} = 1{,}34\ ppm$$

Hence, 1,34 ppm is the concentration of IMD adsorbed to SBA-15, starting from 5 ppm IMD, so a 27 % adsorption takes place. The reason for such low adsorption yield has been explained previously (see above).

The slow desorption of IMD from SBA-15 starting at 90 minutes could be explained by a change in pH (following dissolution of CO_2).

At this point it was decided to discontinue the use of SBA-15 based on the low adsorption observed, on the slow desorption takin place with time, and on the fact that SBA-15 powder was not easy to separate from solution after the experiments.

- TiO₂/Cu

The experimental procedure was described previously in the Materials and Methods section. The UV/Vis spectra of the samples are shown in **Figure 9.**
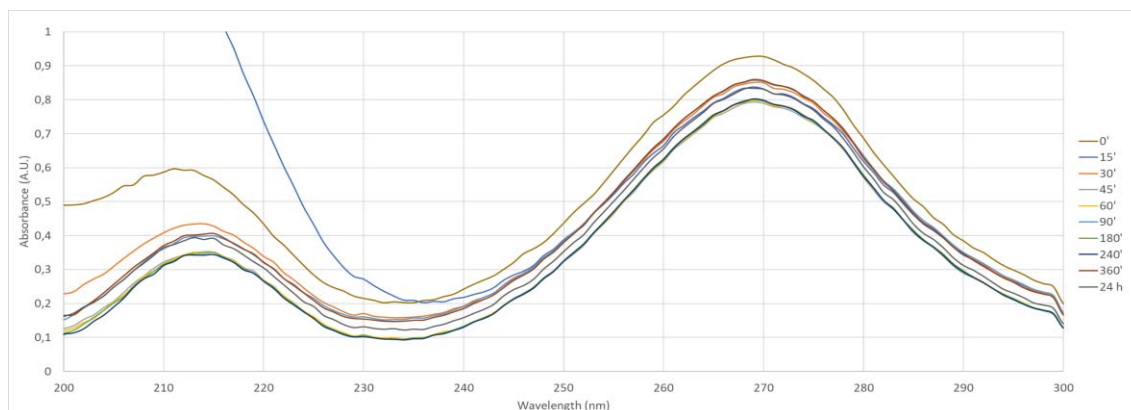

Figure 9.- *Time-resolved spectra of IMD adsorption over TiO₂/Cu. [IMD] = 10 ppm, [TiO₂/Cu] = 30 ppm, pH=7, 25ºC*

As in the previous experiment, the variation of absorbance with time was monitored at λ=270 nm and 214 nm to study the adsorption process, as depicted in **Figure 10.**

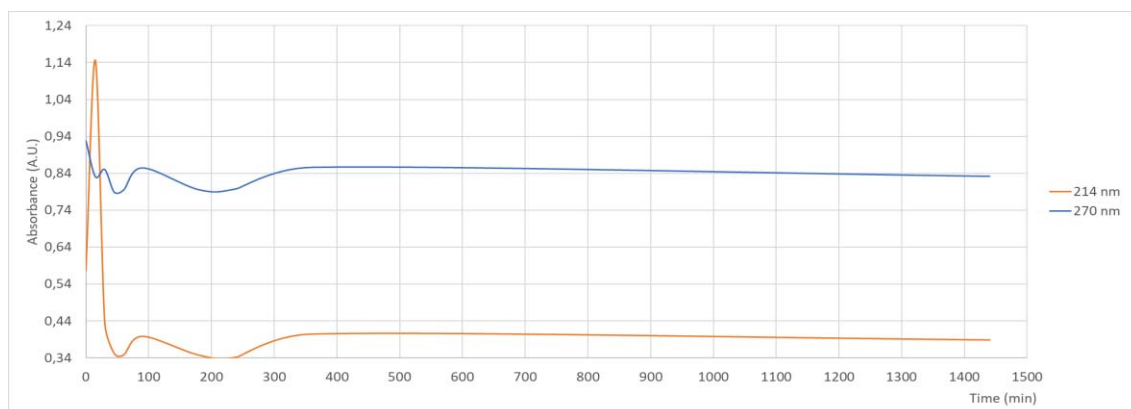**Figure 10.-** *Evolution of absorbance of IMD at maxima λ=270nm and λ=214nm. [IMD] = 10 ppm, [TiO₂/Cu] = 30 ppm, pH=7, 25ºC*

Figure 10 shows a slight decrease of approximate 10% in absorbance for the 270 nm maximum after 15 min. A greater decrease (32%) is seen for the 214 nm after reaching saturation levels of absorbance during the first 15 min. This experiment was undergone at pH 7,66. The variation of absorbance observed for 214 nm has not been considered for the calculations of IMD adsorbed, since the strong saturation observed during the first 15 minutes of experience, as in the case of SBA-15, cannot correspond to an increase in the concentration of IMD in solution.

Thus, the concentration of IMD adsorbed onto TiO$_2$/Cu, following the decrease in 270 nm, can be estimated as:

$$\Delta Abs = 0,1046[IMD]$$

$$0,13 = 0,1046[IMD]$$

$$[IMD] = \frac{0,13}{0,1046} = 1,24 \; ppm$$

1,24 ppm, with respect to the initial 10 ppm of IMD used in this experience, corresponds to a 12% of maximum IMD adsorbed to TiO$_2$/Cu.

The saturation of absorbance at 214 nm can be mainly due to TiO$_2$/Cu itself. It was previously explained (see above) that small changes in pH or T may lead to variations in absorbance at this wavelength. The pH measured at the beginning of the TiO$_2$/Cu experiment was of 7,7. Absorbance changes at 214 nm during the experiment can be interpreted as a change in pH during the experiment, possibly due to the pK$_a$ differences between TiO$_2$/Cu and IMD.

This change in pH may facilitate liberation of Cu^{+2} ions from the TiO$_2$/Cu surface.

   o   *Lixiviation study of TiO$_2$/Cu*

Following the previous results, the potential lixiviation of Cu^{+2} from the catalyst was tested, as described previously in the Materials and Methods section. ***Table 1*** summarizes the obtained results.

Table 1.- Masses recorded from the lixiviation study of TiO$_2$, 25ºC

	Added mass TiO$_2$/Cu (g)	*Final mass TiO$_2$/Cu (g)*	*% mass lost*	*Avg. %*
24h (1)	0,0245	0,017	30,6	27,7
24h (2)	0,0207	0,0155	25,1	
48h (1)	0,0208	0,0156	25,0	19,6
48h (2)	0,0255	0,0216	15,3	

The average percentage of mass loss was of about 27,7% in 24 h, and 19,6% in 48 h. These values show TiO$_2$/Cu photocatalyst is not mechanically stable under these conditions. Since TiO$_2$ is known to have a very stable crystalline structure, it is reasonable to assume that the lixiviation is due to the loss of Cu, which might be not strongly linked into the crystalline network.

At this point, considering the strong lixiviation observed, it was decided to discontinue the use of this photocatalyst.

- BP50/P25

The experimental procedure was described previously in the Materials and Methods section. All the different proportions of BP50/P25 studied (40:60, 30:70, 20:80 and 10:90) followed the same procedure. The UV/Vis spectra of IMD 5 ppm over 3 pellets (59,6 mg) of BP50/P25 30:70 is shown in *Figure 11*.
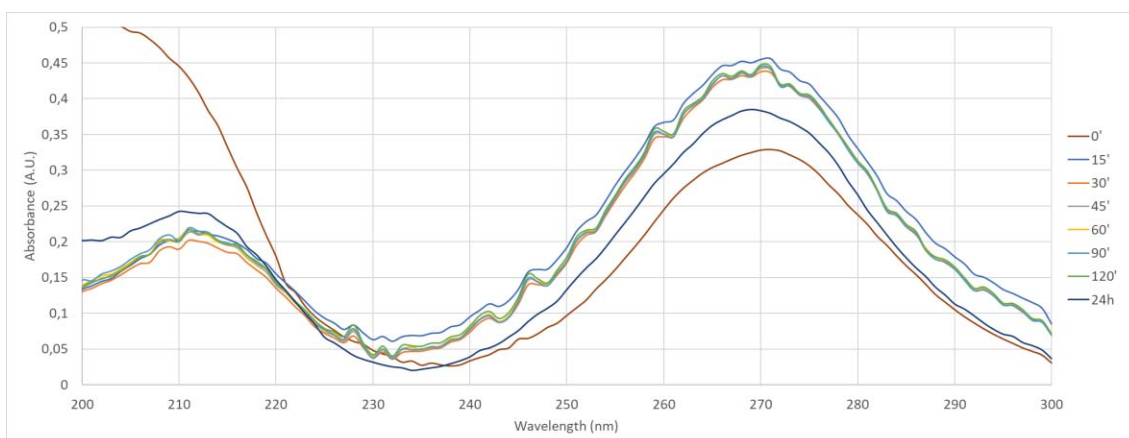

Figure 11.- *Time-resolved spectra of IMD adsorption over BP50/P25. [IMD] = 5 ppm, BP50/P25 quantity = 3 pellets, 30:70 proportion of BP50:P25, 25ºC*

As in previous experiments, the variation of absorbance with time was monitored at λ = 270 nm, 214 nm to study the kinetics of adsorption, as depicted in *Figure 12*.

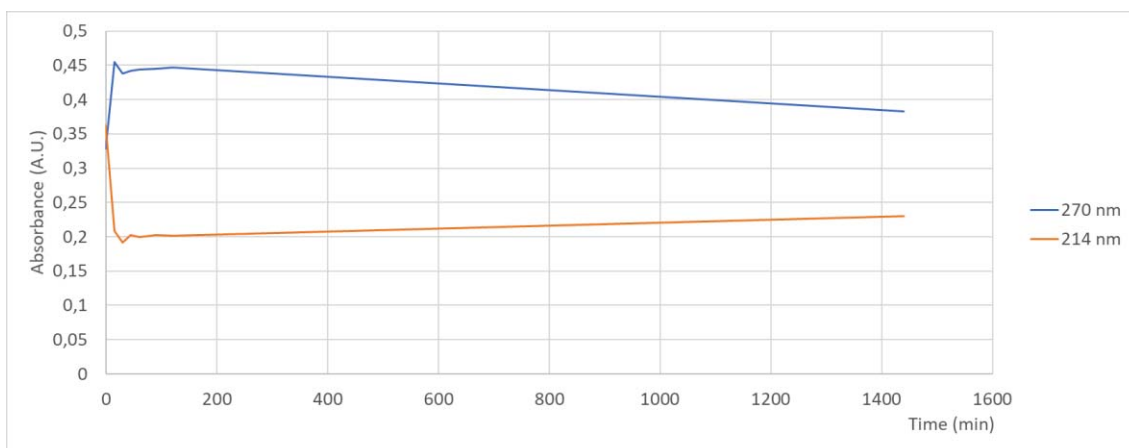**Figure 12.-** *Evolution of absorbance of IMD at maxima λ=270nm and λ=214nm. [IMD] = 5 ppm, BP50/P25 quantity = 3 pellets, 30:70 proportion of BP50:P25, 25ºC*

We have previously mentioned that the 214 nm maximum cannot be used in some cases, since it is heavily influenced by pH changes. Nevertheless, in this case the 270 nm maximum also suffers an increase starting from t=0. Therefore, the 270 nm wavelength

cannot be monitored to calculate the approximate concentration of IMD adsorbed to the photocatalyst. BP50/P25 contains clays and TiO_2/Cu **[19]**. Both components have a basic nature, hence they get easily protonated. Therefore, the observed behavior can be rationalized in terms of a very low adsorption of IMD on BP50/P25.

As in the case of both SBA-15 and TiO_2/Cu, absorbance changes at 214 nm and 270 nm during the present study can be interpreted as a change in pH during the experiment, possibly due to the relation between the isoelectric point (pI) of BP50/P25 and the pK_a of IMD.

It can also be inferred from these experiments that both chromophores responsible for the 214 and 270 nm behave differently depending on the pH conditions and the nature of the photocatalyst. In this case, the pH at the beginning and end of the experiment kept constant at *ca.* 4 in all cases. As previously, changes in the pH of the experiment could be inferred by comparison of the absorbance values of the 214 nm maximum after 120 min to those of the different pH calibrations. Further, the absorbance at 270 nm for each experiment at 120 min will be also analyzed in a similar way to infer whether the chromophore responsible for this maximum also undergoes changes due to the pH.

Table 2.- Comparison of absorbances values observed for IMD with the different BP50/P25 pellets studied and the pH 4 and pH 9 calibrations. l = 214, 270 nm

	pH 4 calibration	pH 9 calibration	BP50/P25 40:60	BP50/P25 30:70	BP50/P25 20:80	BP50/P25 10:90
214 nm Absorbance (A.U.)	0,36	0,17	0,09	0,20	0,33	0,30
270 nm Absorbance (A.U.)	0,33	0,44	0,44	0,45	0,41	0,38

Analysis of the absorbance values in Table 1***Table 2*** shows that during the experiment there is a variation in pH. For example, for the BP50/P25 20:80, 40:60 and 10:90, the absorbance values at 270 nm after 120 min show absorbances similar to those at pH 9.

As discussed previously (***SBA-15 section***), the functional groups responsible of the two pK_a of IMD were found as nitrogen groups. These N atoms have electrons located on antibonding MOs, which can easily undergo protonation. Thus, in this case, these groups are responsible for the variation of absorbance at 270 nm due to changes in pH that interfere with these electrons.

The experimental procedure was described previously in the Materials and Methods section. The last pellets of BP50/P25 studied were composed of 90% BP50 and 10% of P25, although they come from a different batch than the previous 10:90 pellets. This experiment was performed twice: at pH 4 and pH 6,8. The UV/Vis spectra of the samples are shown in **Figure 13** and **Figure 14**. The pH of all experiments using BP50/P25 was pH *ca.* 4. An experiment was carried out at pH 6,8 using a $KHPO_4/K_2PO_4$ buffer.

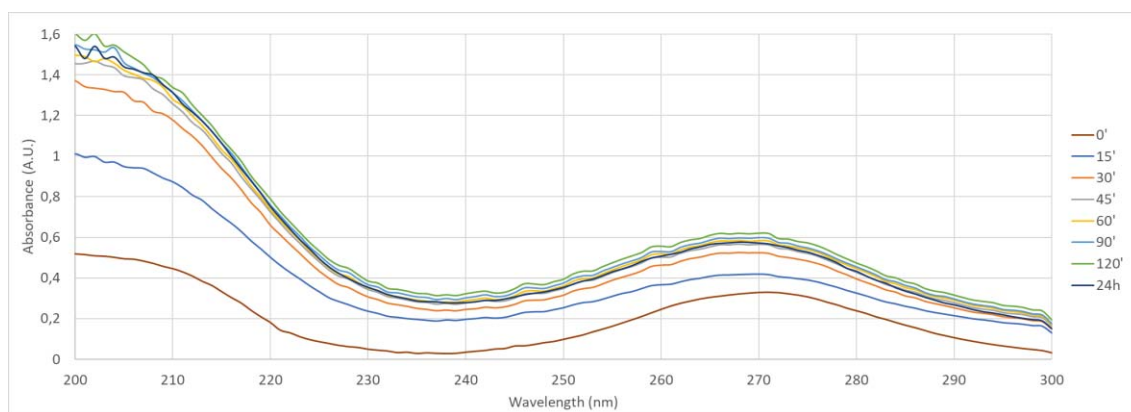**Figure 13.-** *Time-resolved spectra of IMD adsorption over BP50/P25. [IMD] = 5 ppm, BP50/P25 quantity = 3 pellets, pH=4, 25ºC*

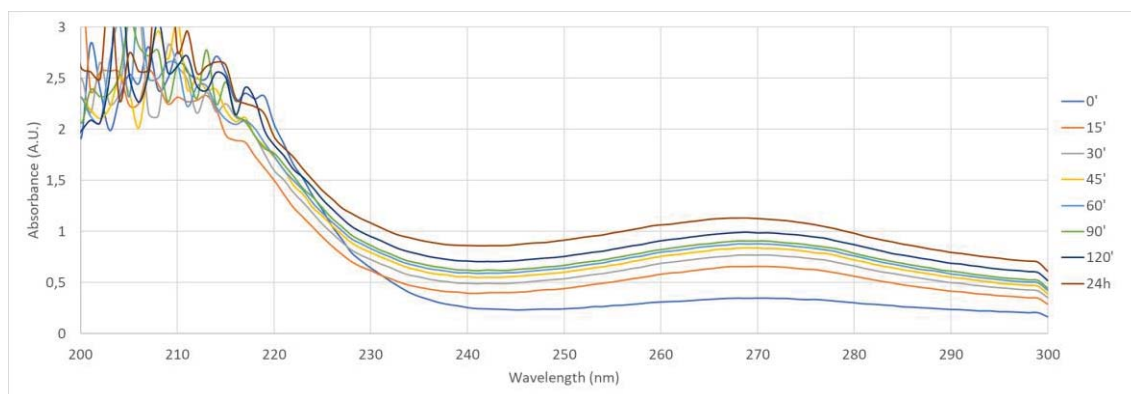**Figure 14.-** *Time-resolved spectra of IMD adsorption over BP50/P25. [IMD] = 5 ppm, BP50/P25 quantity = 3 pellets, pH=6,8; 25ºC*

The variation of absorbance with time was monitored at λ = 270 nm, 214 nm in order to study the kinetics of adsorption, as depicted in **Figure 15** and **Figure 16.**

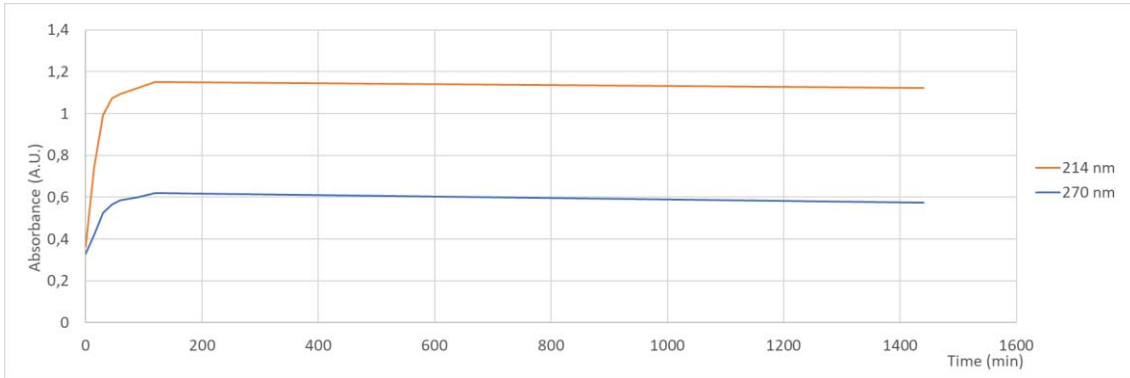**Figure 15.-** *Evolution of absorbance of IMD at maxima λ=270nm and λ=214nm. [IMD] = 5 ppm, BP50/P25 quantity = 3 pellets, pH=4, 25ºC*
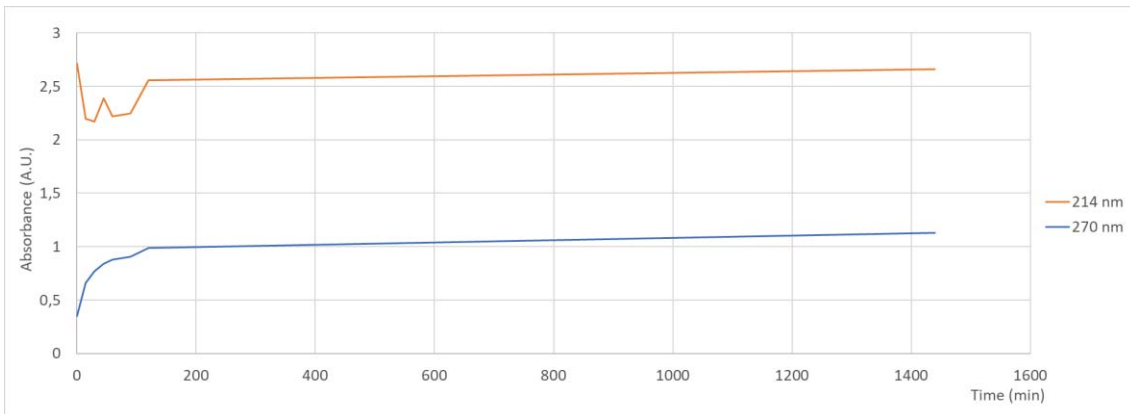
Figure 16.- *Evolution of absorbance of IMD at maxima λ=270nm and λ=214nm. [IMD] = 5 ppm, BP50/P25 quantity = 3 pellets, pH=6,8; 25ºC*

The general trend on both 214 and 270 nm maxima showed an increase in absorbance, with an increase of 0,79 A.U. at 214 nm and an increase of 0,29 A.U. at 270 nm Therefore, changes in absorbance at 214 nm can be interpreted based on pH changes in solution. Therefore, these values cannot be used to monitor changes in [IMD] due to adsorption onto the photocatalyst.

The experiment was repeated at pH = 6,8 using a $KHPO_4/K_2PO_4$ buffer. The observed 214 nm absorbances were all close to 2 A.U., meaning that the spectrophotometer's detector is saturated at this wavelength. This can be attributed to the presence of the $KHPO_4/K_2PO_4$ buffer. The trend at 270 nm shows an increase of 0,78 A.U., that can be explained on the basis of the differences in absorbance at different pH values, as previously. Therefore, this batch of BP50/P25 has not shown any clear adsorption of IMD on its surface from the 4-7 pH range.

Photolysis of IMD

The experimental procedure was described previously in the Materials and Methods section. ***Figure 17*** shows the absorbance value of each sample at the maximum of IMD (270 nm).
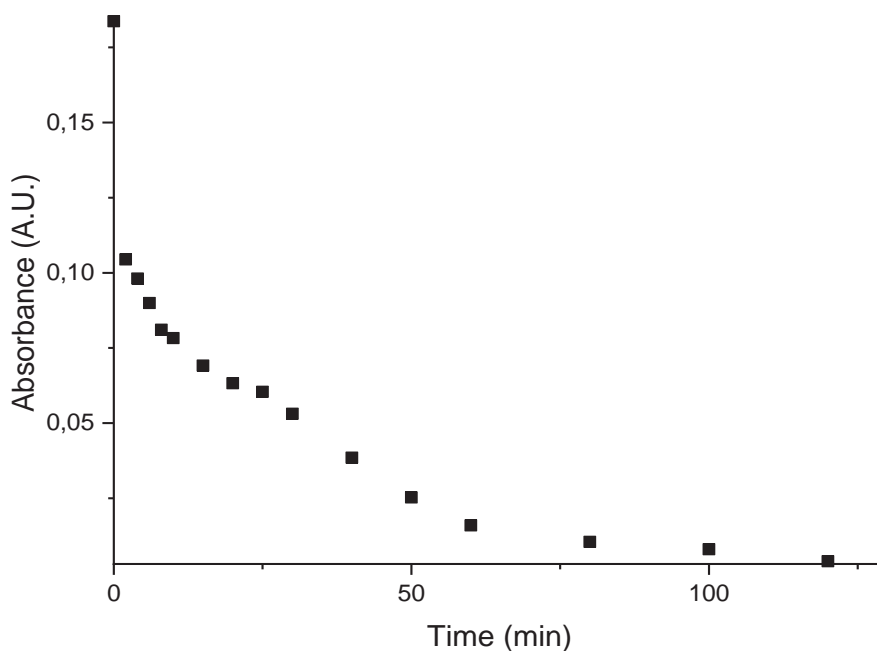

Figure 17.- *Absorbance evolution of IMD photolysis through time under UV light (254 nm)*

The results shown in ***Figure 17*** can be interpreted as IMD being clearly degraded by UV light (254 nm) through photocatalysis. In order to infer whether the reaction corresponds to a single process or a set of two consecutive processes, the observed results were fit to a first order decay and to two consecutive first order decays. Non-linear curve fitting was used for this, using *OriginPro 2019b*. ***Figure 18*** and ***Figure 19*** display the results obtained for both fittings.
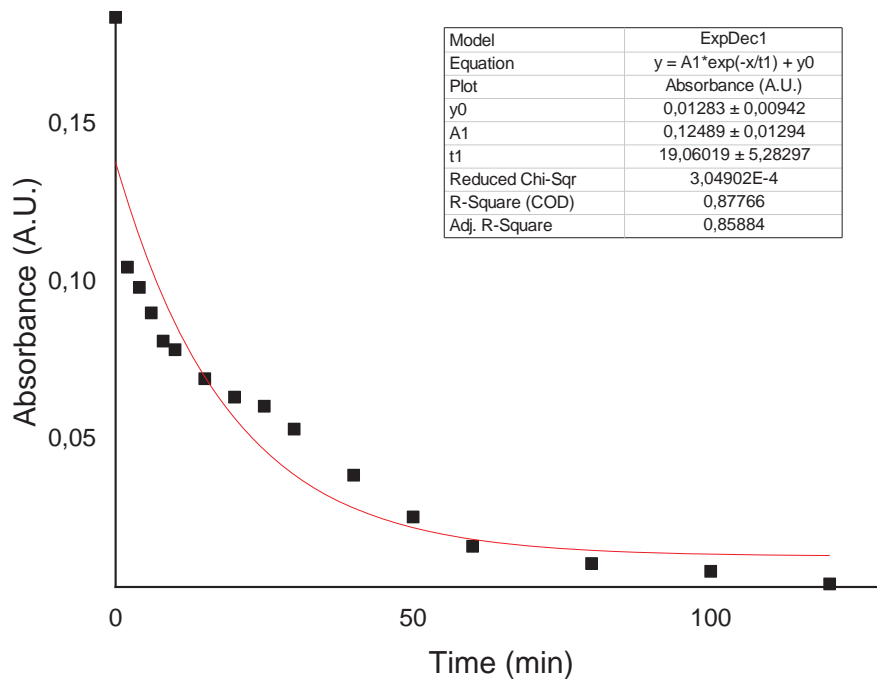
Model	ExpDec1
Equation	y = A1*exp(-x/t1) + y0
Plot	Absorbance (A.U.)
y0	0,01283 ± 0,00942
A1	0,12489 ± 0,01294
t1	19,06019 ± 5,28297
Reduced Chi-Sqr	3,04902E-4
R-Square (COD)	0,87766
Adj. R-Square	0,85884

Figure 18.- *First order decay exponential fitting of the photolysis results*

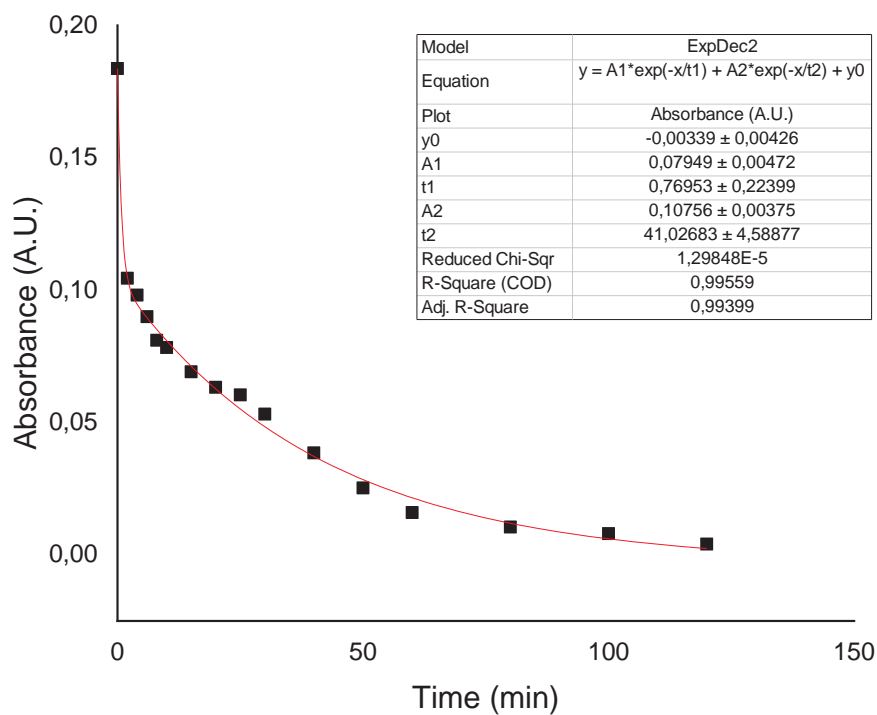| Model	ExpDec2
Equation	y = A1*exp(-x/t1) + A2*exp(-x/t2) + y0
Plot	Absorbance (A.U.)
y0	-0,00339 ± 0,00426
A1	0,07949 ± 0,00472
t1	0,76953 ± 0,22399
A2	0,10756 ± 0,00375
t2	41,02683 ± 4,58877
Reduced Chi-Sqr	1,29848E-5
R-Square (COD)	0,99559
Adj. R-Square	0,99399

Figure 19.- *Two consecutive first order decay exponential fitting of the photolysis results*

The following equations were used:

$$y = A * exp^{\left(-\frac{x}{t1}\right)} + y0$$

$$y = A1 * exp^{\left(-\frac{x}{t1}\right)} + A2 * exp^{\left(-\frac{x}{t2}\right)} + y0$$

Where "y" is the absorbance, A_n is related to the initial and infinite time absorbance, and t_n the inverse of the decay constant of the reaction (k), i.e., the natural lifetime, $k = 1/t$. The fitting to a biexponential decay is clearly better, both from the point of view of the residuals of the fit and also based on the R^2 values. Thus, this second fitting value can be interpreted as IMD following a biphasic photolytic degradation process, with a fast process followed by a slower one, both responding to a first order kinetic model.

In view of these results, the data were studied separately in order to estimate the values of the k_1 and k_2 constants more accurately. For that, the experiments were also performed for 2 hours, but the first 10 min and the rest of the process were fitted separately.

Further, the potential involvement of IMD excited triplet state was considered. For that, the photolysis of IMD was performed in both 100% O_2 atmosphere and 100% N_2 atmosphere. It is well known that, in molecular oxygen, there are 16 electrons can be ordered in such a manner that there is a double bond between both O atoms. This electron configuration shows that the outer most molecular orbital (π^*_{2p}) is only half-filled. In this electronic configuration, there are three different states corresponding to different arrangement of these electrons, which ae $^3\Sigma^+_g$, $^1\Delta_g$, and $^1\Sigma^*_g$. The ground-state of molecular oxygen is the triplet state ($^3\Sigma^+_g$); therefore, molecular oxygen is really a bi-radical in its groud state. Thus, many reactions of O_2 ($^3\Sigma^+_g$) with species that are singlets in their ground state are experimentally very slow, due to a quantum restriction of chemical reactivity, even if they are strongly favored by thermodynamics [20].

Hence, having determined both k_1 and k_2 constants calculated in both atmospheres, it can be assumed whether IMD is in a triplet or a singlet spin multiplicity state when excited with UV light. **Table 3** displays the calculated k_1 and k_2 constants in normal atmosphere, 100% O_2 atmosphere, and 100% N_2 atmosphere.

Table 3.- Comparison of k_1 and k_2 obtained in 21% O_2, 100% O_2, and 100% N_2

Constant (s^{-1})	Air-satd. Atmosphere (21% O_2)	100% O_2	100% N_2
k_1	0,011 ± 0,003	0,015 ± 0,001	0,008 ± 0,001
k_2	$4{,}0 \cdot 10^{-4} \pm 0{,}6 \cdot 10^{-4}$	$5{,}3 \cdot 10^{-4} \pm 0{,}7 \cdot 10^{-4}$	$5 \cdot 10^{-4} \pm 1 \cdot 10^{-4}$

The results shown in **Table 3** can be interpreted as IMD* being very reactive with O_2. As shown in Table 2, there is still reaction in the absence of O_2 (100% N_2), where k_1 is half of its value in 100% O_2. This means that both the triplet (^{3}IMD) and singlet (^{1}IMD) states

of IMD participate in the initial deactivation process. As expected, k_2 is not influenced by the presence of O_2, as the excited state of IMD has already relaxed in the first process. The observed k_2 values are compatible from a statistical point of view, and the second process is much slower than the first one.

IMD* undergoes an intersystem crossing (ISC) from a singlet state to the triplet state before reacting. This implies that the activation energy (E_a) of the photoreaction taking place from ^{1}IMD is lower than the activation energy from ^{3}IMD. In other words, the process taking place from the singlet state is kinetically favored.

The fact that similar values of k_2 are observed gives also relevant information on the reaction mechanism. It can be assumed that IMD*, either in triplet or singlet state, react and degrade into different products. Afterwards, these products undergo a second reaction and transform into different new photoproducts. IMD photolysis take place as follows (**Figure 20**):
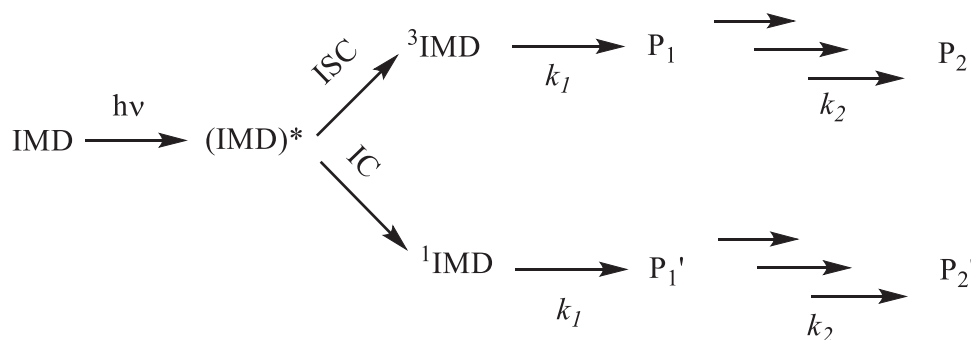

Figure 20.- *Proposed degradation mechanism of IMD under UV light (λ=254nm)*

In parallel to these experiments, samples at different times of IMD photolysis were analyzed by HPLC, in order to monitor the degradation of the pesticide in 21% O_2 atmosphere, 100% O_2, and 100% N_2.

Figure 21 shows the chromatograms obtained at different times during the reaction at 100% O_2 atmosphere. At the beginning of the process, only IMD is present, during the process different intermediates are observed and at 60 min these have partially disappeared. We have monitored the areas of the peaks and calculated the degradation percentage for IMD and for two possible photoproducts (PP1 and PP2) under 21% O_2 according to the following equation:

$$Degradation\ \% = \frac{Area\ of\ compound\ at\ t = 0 - Area\ of\ compound\ at\ t = x}{Area\ of\ compound\ at\ t = 0} * 100$$
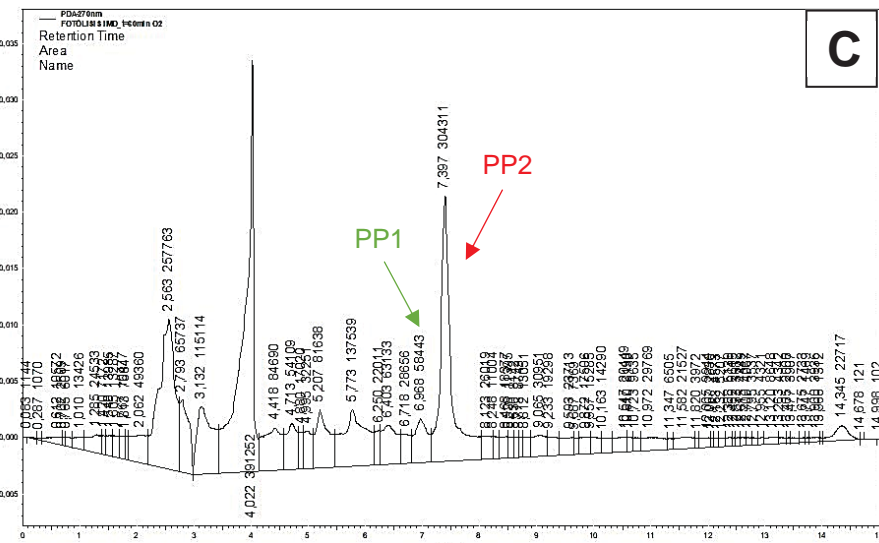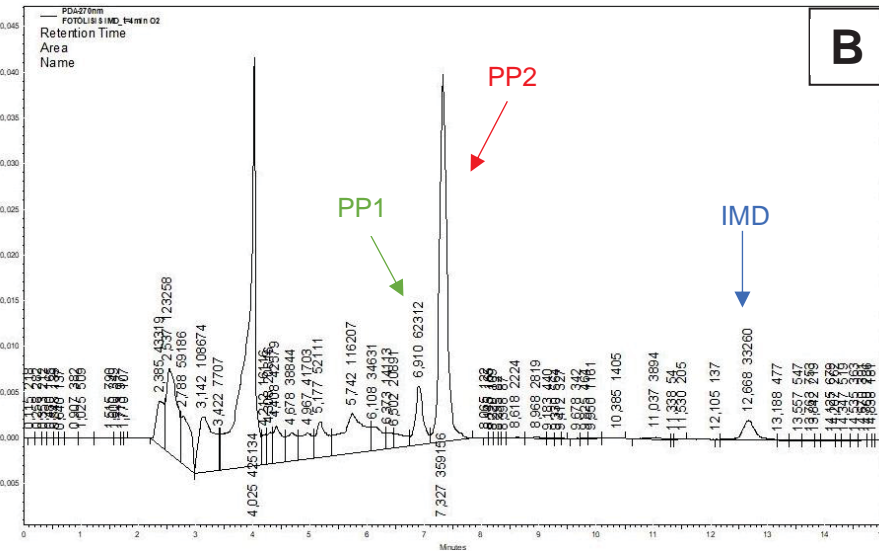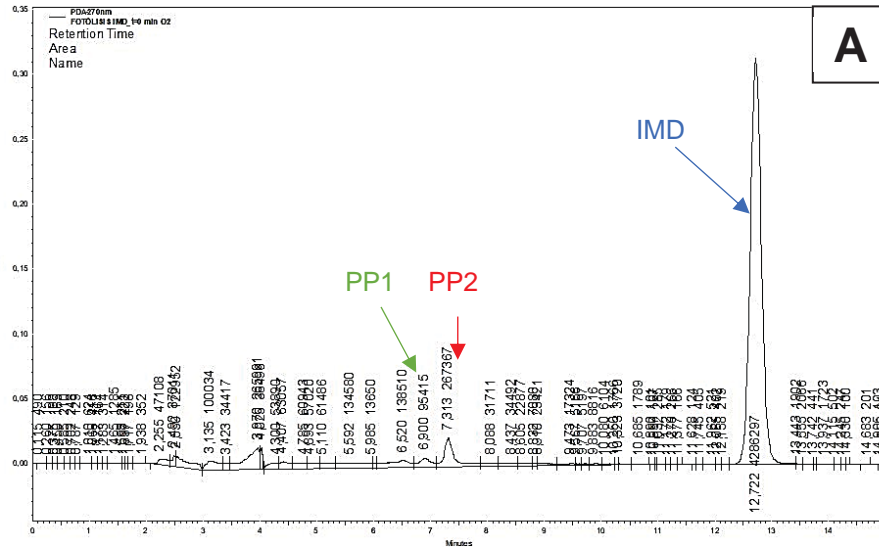
Figure 21.- *Chromatograms of IMD 5 ppm just after irradiation starts (A) at t=4 min (B), and at t=60 min (C) in 100% O_2 atmosphere. IMD, PP1 and PP2 highlighted on the figure.*

The results obtained are displayed in **Table 4,** and **Figure 22** depicts the degradation of each compound relative to their maximum concentration.

Table 4.- Chromatogram areas of IMD, PP1 and PP2 and % of degradation of each compound at different UV light irradiation times. 21% O_2 atmosphere.

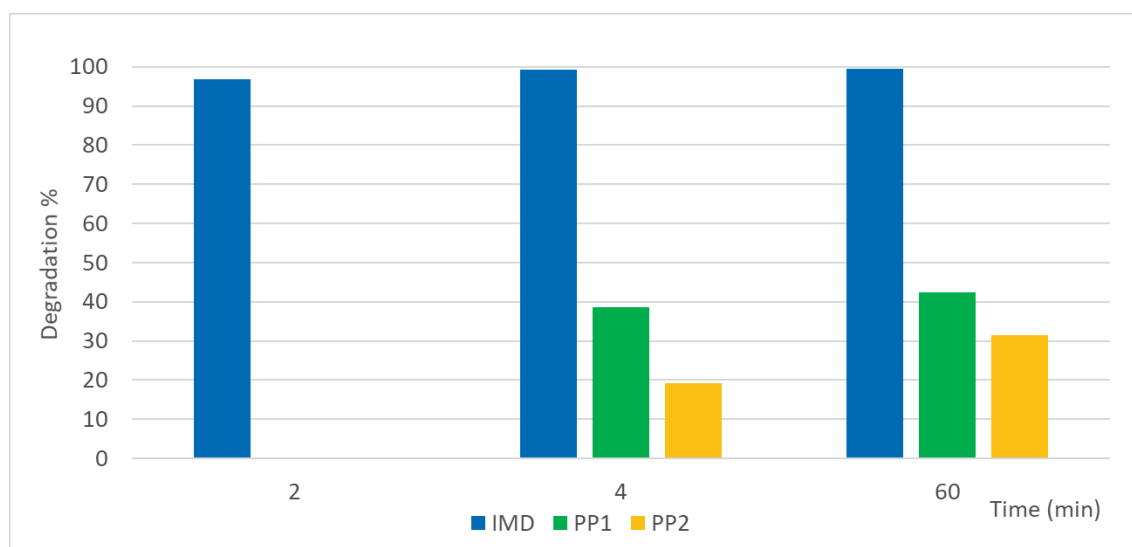| Sample time (min)	Area IMD	Degradation % IMD	Area PP1	Degradation % PP1	Area PP2	Degradation % PP2
Irradiation starts	4286297	---	95415	---	267367	---
2	130997	96,9	101593	---	444007	---
4	33260	99,2	62312	39	359156	19
60	22717	99,5	58443	43	304311	32

Figure 22.- *% of degradation of IMD, PP1, and PP2 at different times or UV light irradiation relative to their maximum concentration. 21% O_2 atmosphere.*

From these results, IMD undergoes a very fast degradation under 21% O_2, more than 90% of it being degraded during the first 2 min and achieving almost complete degradation after 60 min of UV irradiation. These results are in agreement with the observed rate constants, given that k_1 indicated a very fast degradation during the first 10 min of reaction, while k_2 proved a slow and steady degradation process after 10 min.

From **Table 4**, both PP1 and PP2 are formed as soon as the sample is irradiated with UV light. The observed areas (which can be interpreted as "concentrations") for PP1 and PP2 (**Table 4**) reach their maximum at t=2 min in both cases. The results in **Table 4** also prove the degradation of PP1 under UV light, having a slow decay after 4 min of irradiation (38,7%), achieving a slightly greater degradation after 60 min (42,5%). Another possible photoproduct (PP2) is observed to start forming after 2 min of UV light exposure. As in the case of PP1, this product also shows degradation, achieving a decay of 31,5% after 60 min. The simultaneous disappearance of both corresponds to the slow

second process with rate constant k2.

The results obtained are displayed in **Table 5** and **Figure 23** depicts the degradation of each compound relative to their maximum concentration.

Table 5.- Chromatogram areas of IMD, PP1 and PP2 and % of degradation of each compound at different UV light irradiation times. 100% O_2 atmosphere.

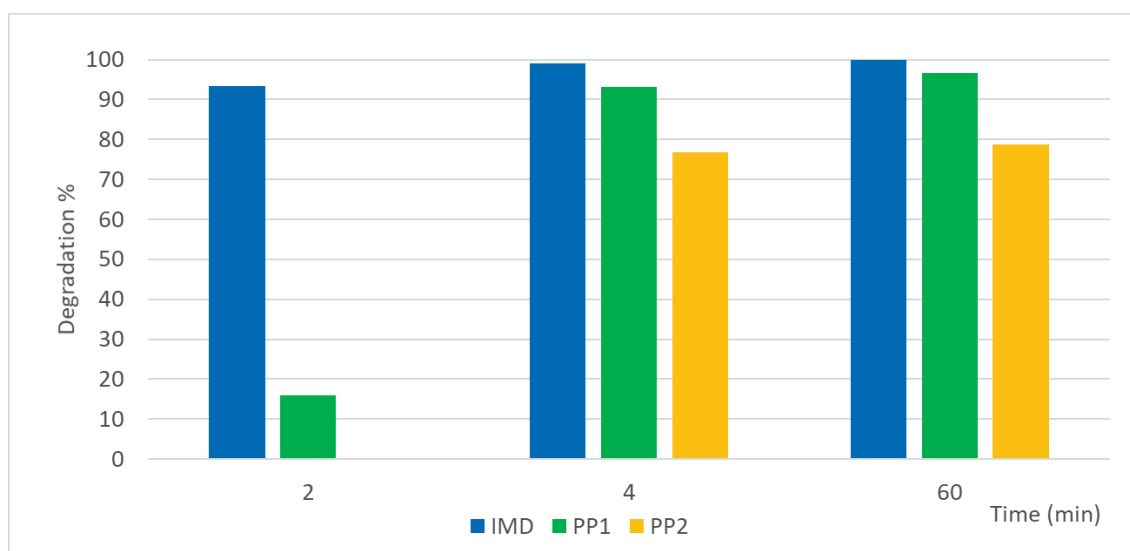| Sample time (min)	Area IMD	Degradation % IMD	Area PP1	Degradation % PP1	Area PP2	Degradation % PP2
Irradiation starts	762125	---	79922	---	0	---
2	51124	93,3	67190	15,9	195482	---
4	7071	99,1	5417	93,2	45459	76,7
60	350	99,9	2708	96,6	41674	78,7

Figure 23.- *% of degradation of IMD, PP1, and PP2 at different times or UV light irradiation relative to their maximum concentration. 100% O_2 atmosphere.*

From these results, IMD undergoes a very fast degradation under 100% O_2 atmosphere, >90% of it being degraded during the first 2 min and achieving almost complete degradation after 60 min of UV irradiation. These results are in agreement with the obtained k_1, that showed a fast degradation during the first 10 min of reaction.

The results also indicate the presence of PP1 as soon as IMD irradiation starts. The results in **Table 5** also prove the degradation of PP1 under UV light, having a slow decay (k_2) after 2 min of irradiation (15,9%), and achieving the highest level of degradation after 60 min (96,6%). A PP2 is observed to start forming after 2 min of UV light exposure. As in the case of PP1, this product also shows degradation (k_2), achieving a great decay of 78,7% after 60 min.

Samples obtained from UV photolysis under 100% N_2 were also analyzed by HPLC. **Table 6** shows the area of the most relevant peaks seen in each sample and the degradation percentage observed for IMD and two possible photoproducts (PP1 and PP2) under these conditions. **Figure 24** depicts the degradation of each compound relative to their maximum concentration.

Table 6.- Chromatogram areas of IMD, PP1 and PP2 and % of degradation of each compound at different UV light irradiation times. 0% O2 atmosphere.

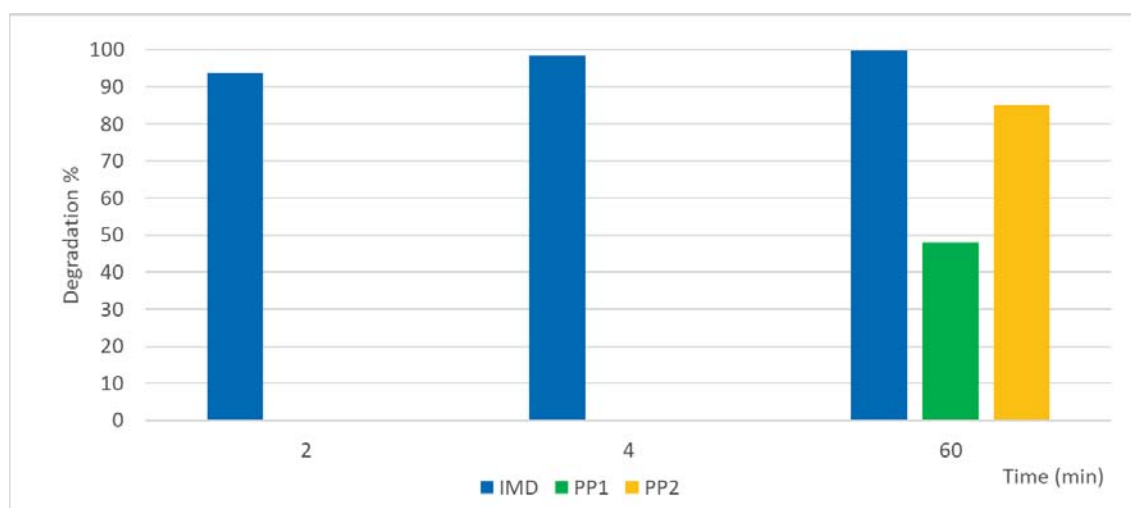| Sample time (min)	Area IMD	Degradation % IMD	Area PP1	Degradation % PP1	Area PP2	Degradation % PP2
Irradiation starts	5297738	---	212919	---	0	---
2	328834	93,8	332765	---	74742	---
4	85698	98,4	359355	---	84575	---
60	9230	99,8	186896	48,0	12591	85,1

Figure 24.- *% of degradation of IMD, PP1, and PP2 at different times or UV light irradiation relative to their maximum concentration. 0% O₂ atmosphere.*

From the results displayed in **Table 6**, it can be assumed that IMD undergoes fast degradation under 100% N_2 atmosphere more than 90% of it being degraded during the first 2 min and achieving almost complete degradation after 60 min of UV irradiation. These results are in agreement with the observed k_1, that showed a fast degradation during the first 10 min of reaction. Nevertheless, the constants calculated for 21% O_2 and 100% O_2 proved a faster decay under these conditions than 100% N_2, which indicates a different nature for the states from which reactivity is originated.

In this case, PP1 is also formed upon irradiation, PP2 starts to appear only after 2 min. Further, the areas observed for PP1 and PP2 (**Table 6**) do not reach their maximum until 4 min in both cases. These results are in agreement with the observed k_2.

Photocatalysis of IMD

The experimental procedure was described previously in the Materials and Methods section. **Figure 25** shows the absorbance value of each sample at the maximum of IMD (270 nm).
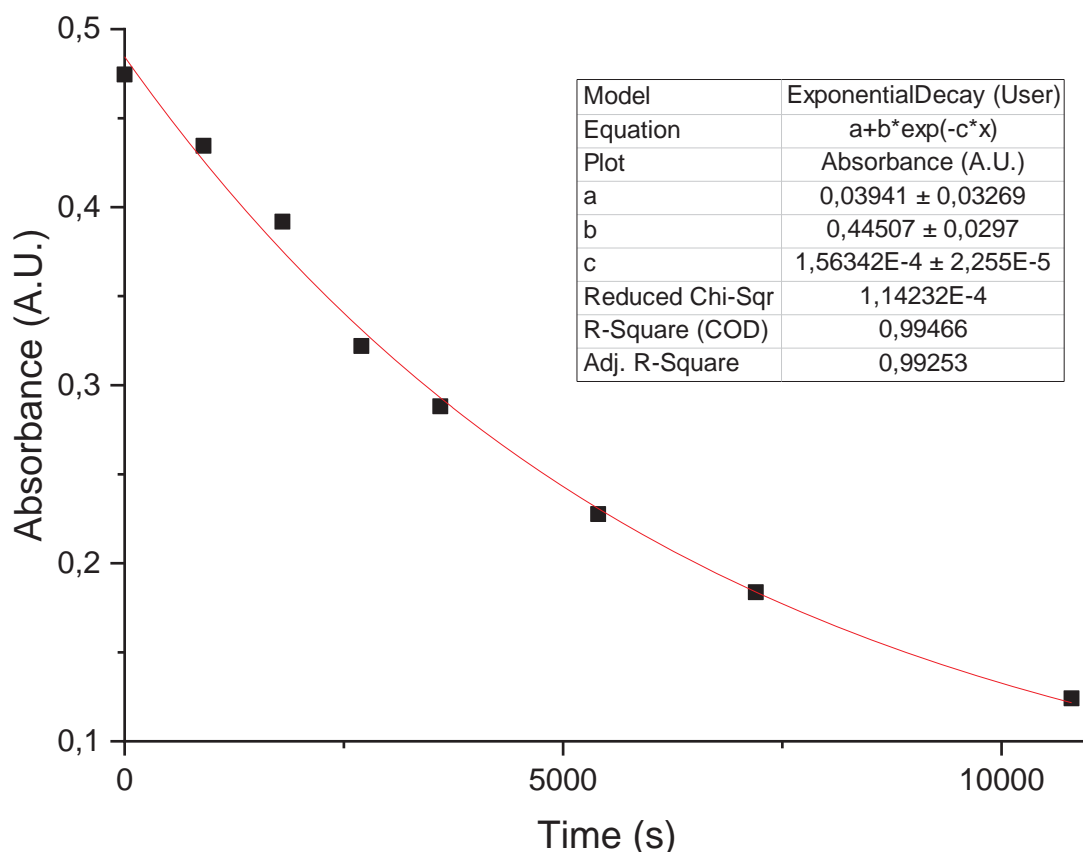
Model	ExponentialDecay (User)
Equation	a+b*exp(-c*x)
Plot	Absorbance (A.U.)
a	0,03941 ± 0,03269
b	0,44507 ± 0,0297
c	1,56342E-4 ± 2,255E-5
Reduced Chi-Sqr	1,14232E-4
R-Square (COD)	0,99466
Adj. R-Square	0,99253

Figure 25.- *Absorbance evolution of IMD photocatalysis through time with BP50/P25 pellets under solar light. Results fitted to a first order decay exponential.*

Figure 25 shows the data obtained, appropriately fitted using a first order kinetic model. The decay constant *k* was calculated as $(1,6\pm0,2)\cdot10^{-4}$ s^{-1}, two orders of magnitude smaller than k_1 for IMD photolysis under any of the studied conditions. This means that IMD photodegradation follows a slower process in photocatalysis with BP50/P25 than what was observed upon photolysis. To rationalize this we have to remember that we have discarded the possibility of heterogeneous photocatalysis based on the absence of adsorption. Also, IMD does not absorb sunlight, hence will not undergo direct photolysis under these conditions. Therefore, the only possibility remaining is that the amount of Fe^{2+} present in the catalyst support induces a heterogeneous photo-Fenton process in which HO$^{\bullet}$ radicals are formed.

Under irradiation (λ=300 nm), Fe^{3+} complexes can generate Fe^{2+} and $HO^{\bullet}$ radicals according to [21]:

$$Fe(OH)^{2+} + h\nu \rightarrow Fe_{(aq)}^{2+} + HO^{\bullet}$$
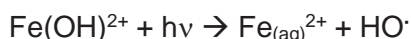
These $HO^{\bullet}$ radicals may react with IMD inducing degradation. The amount of $HO^{\bullet}$ formed in the photo-Fenton process is much lower than the concentration of [IMD] so the reaction is observed a pseudo-first order. The nature of the process observed in this case is completely different from the nature of the process observed upon photolysis. Hence, the observed rate constants are very different, as well.

Characterization of IMD photoproducts

The experimental procedure was described previously in the Materials and Methods section. ***Figure 26*** shows a typical HPLC-MS chromatogram and the corresponding MS spectra obtained from the sample *IMD FL O_2* just after the irradiation starts. As an example of the analysis of the results, IMD shows a peak with 4,833 min retention time (Rt), for which a 278 m/z peak (with 35% relative intensity) is observed in the MS spectra. IMD has a molecular mass of 255 g/mol, the 278 m/z resulting from the formation of an adduct between IMD and Na^+. Additionally, the mass spectra show two other peaks with greater relative intensity (m/z, %): 175 ($C_9H_{10}N_4$, 68%), 209 (67%), in agreement with previous work by [22].
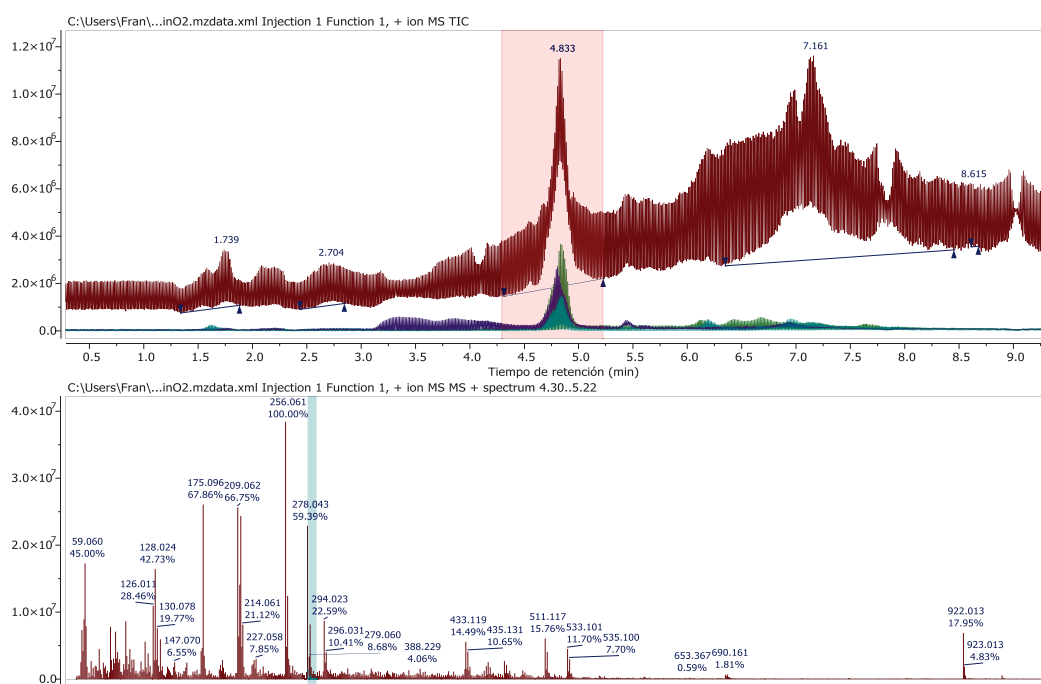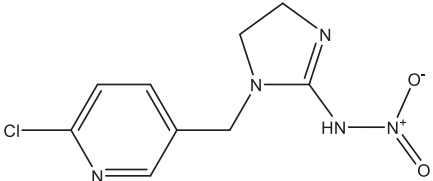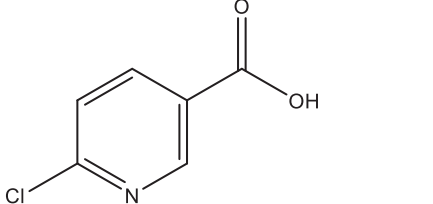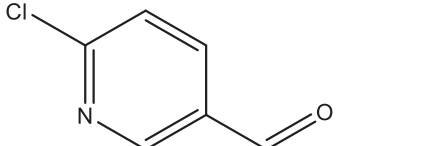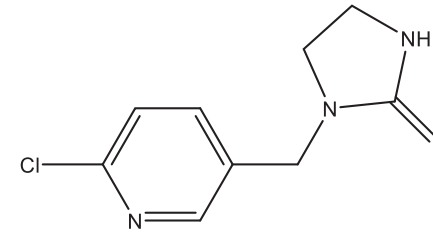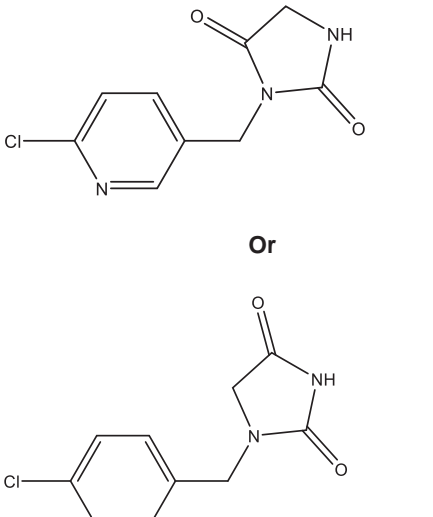

Figure 26.- *HPLC-MS chromatography (above) and masses spectrometry (below) of IMD photolysis just after irradiation starts under 100% O_2 atmosphere.*

Additional samples were obtained under O_2 atmosphere, and their photoproducts identified. Based on the literature, potential photoproducts expected for this reaction were: 6-chloronicotinic acid **(2),** 6-chloronicotinaldehyde **(3),** IMD urea **(4),** IMD keto-urea **(5),** IMD N-nitroso imine **(6),** IMD imine (**7**), IMD imine olefin **(8),** and IMD hydroxy **(9)** **[22][23][24].** The structures, molecular formula, and molecular weight of both IMD and its potential photoproducts are shown in **Table 7**.

Table 7.- Structures, molecular formula, and molecular weight of IMD (1), 6-chloronicotinic acid (2), 6-chloronicotinaldehyde (3), IMD urea (4), IMD keto-urea (5), IMD N-nitroso imine (6), IMD imine (7), IMD imine olefin (8), and IMD hydroxy (9)

	Molecular structure	Molecular formula	Molecular weight (g/mol)
1		$C_9H_{10}ClN_5O_2$	255,66
2		$C_6H_4ClNO_2$	157,55
3		C_6H_4ClNO	141,55
4		$C_9H_{10}ClN_3O$	211,65
5	Or	$C_9H_8ClN_3O_2$	225,63

#	Structure	Formula	Mass
6		$C_9H_{10}ClN_5O$	239,66
7		$C_9H_{11}ClN_4$	210,67
8		$C_9H_9ClN_4$	208,65
9		$C_9H_{11}ClN_5O_3$	272,66

Table 8 shows the presence of IMD and the different photoproducts identified in each sample.

Table 8.- Retention times of the compounds identified in the mass spectrometry spectra of IMD photolysis under UV light and 100% O_2.

Sample (min)	Retention time (min); m/z (adduct, intensity%)				
	1	4	5	6	9
0	4,82; 278 (Na⁺, 35%)	4,81; 212 (H⁺, 34%)	---	4,82; 278 (K⁺, 31%)	4,83; 294 (Na⁺, 12%)
2	4,85; 256 (H⁺, 19%)	4,81; 212 (H⁺, 59%)	2,11; 243 (NH₄⁺, 7%)	4,84; 278 (K⁺, 14%)	---
4	---	4,82; 212 (H⁺, 91%)	2,12; 243 (NH₄⁺, 9%)	---	---
60	---	---	---	---	---
120	---	---	---	---	---

From the observed results, **2**, **3** and **8** are not observed as photoproducts of IMD photolysis. **1**, **4**, **6** and **9** are observed just after irradiation. This shows **1** photodegradation is very fast, leading to intermediate photoproducts **4**, **6** and **9**, that keep reacting. **9** is formed by hydroxylation onto the pyridine ring, a widely known reaction

route **[25]**. Upon N-O bond breaking, **1** yields **6** (Rt=4,82 min). Hydrolysis/photohydrolysis of the non-detected intermediate **7** leads to **4**, and subsequent oxidation from the excited state at one of the C atoms vicinal to the N on the imidazol ring yields **5**. This sequence is supported by the fact that photoproduct **4** is already observed just after irradiation starts, while **5** is only observed at t=2 min, showing its formation is less energetically favorable. At t=4 min, **6** has completely disappeared and only **4** and **5** remain in solution. These two photoproducts are expected to keep degrading upon further photolysis and would lead via C-C bond scission to **3** and **2**. This last route may also take place directly from **1**. An unidentified peak was observed with (m/z)=59 at all sampled times, reaching its maximum concentration at t=60 min. Potential structures found for this unknown are not compatible with different hypothesis from photodegradation, and it has not been previously reported.

As in the case of the O_2 atmosphere samples, samples under N_2 atmosphere were analyzed. **Table 9** shows the presence of IMD and its different potential photoproducts in each sample.

Table 9.- Retention times of the compounds identified in the mass spectrometry spectra of IMD photolysis under UV light and 0% O_2.

Sample (min)	Retention time (min); m/z (adduct, intensity%)					
	1	4	5	6	9	8
0	4,82; 256 (H+, 62%)	4,80; 212 (H+, 13%)	---	4,84; 278 (K+, 25%)	4,84; 294 (Na+, 6%)	4,83; 209 (H+, 30%)
2	---	4,81; 212 (H+, 90%)	2,12; 243 (NH4+, 9%)	---	---	---
4	---	4,81; 212 (H+, 84%)	2,13; 243 (NH4+, 15%)	---	---	---
60	---	---	---	---	---	---
120	---	---	---	---	---	---

Same as for the O_2 samples, **2**, **3** and **8** are also not present as possible IMD photoproducts in any of the samples studied. Again, **1**, **4**, **6**, and **9** are present just after the irradiation starts, and **5** is observed at t=2 min. Additionally, **8** is also present just after the irradiation starts, being formed by activation of the C atoms that are vicinal to the N atoms on the imidazol ring of **7** (not detected). Again, an unidentified peak was observed with (m/z) = 59 at all sampled times, reaching its maximum concentration at t=60 min.

Figure 27 depicts the proposed photodegradation mechanism of IMD under UV-Vis light.
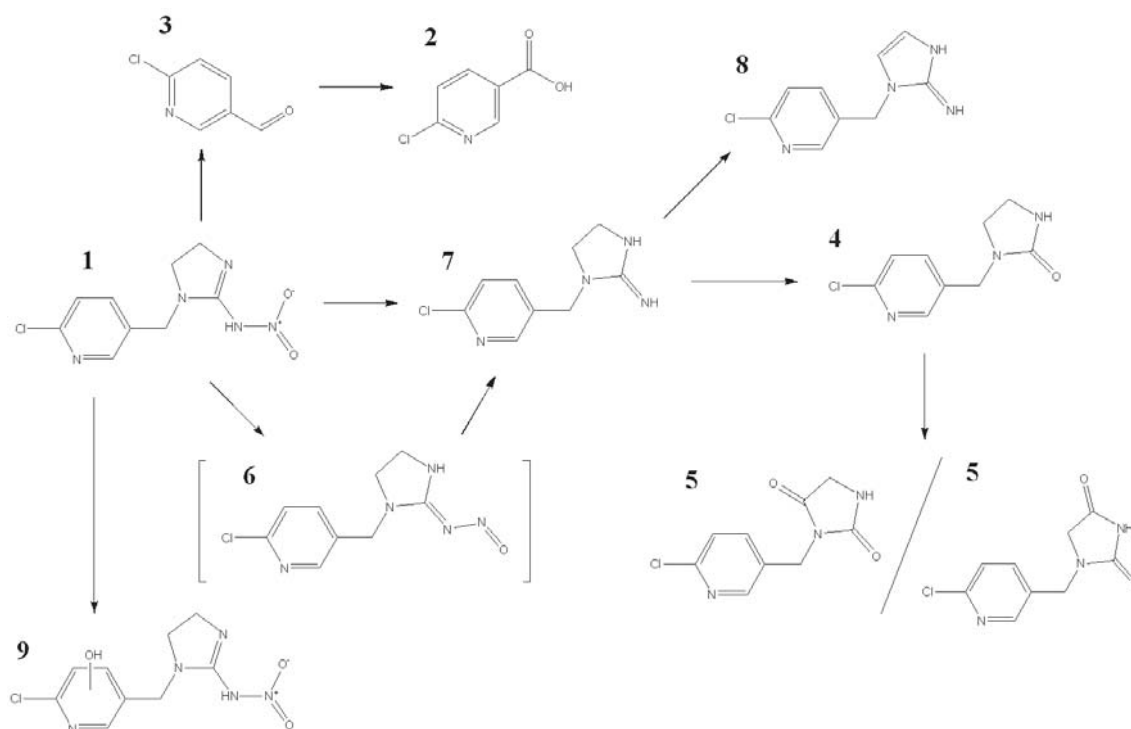

Figure 27.- *Proposed photodegradation mechanism of IMD under UV-light*

Conclusions

During the development of this project, I undertook the study of IMD UV-Vis absorbance, IMD UV direct photolysis, and heterogeneous IMD photocatalysis using BP50/P50 as photocatalysts. This allowed me to train and improve different skills, such as:

- autonomous work
- teamwork
- planning experiments
- decision making
- analysis of experimental results
- use of different software packages for data analysis
- improve my ability to use different apparatus, among these HPLC systems, spectrophotometers, and photoreactors
- use of experimental data plotting and fitting programs

The work had a large interdisciplinary nature, and I had to use concepts and competences from different subjects among those included in the Degree in Chemistry,

such as: organic chemistry, instrumental analytical chemistry, thermodynamics, spectroscopy, surface chemistry and kinetics.

Overall, my degree of satisfaction with this work and its development is very high.

The main findings of this project were as follows:

1. The molar absorption coefficient at natural pH of IMD was 26671 ± 1304 $M^{-1} \cdot cm^{-1}$ at 270nm. The spectrum does not vary with pH.

2. 27% adsorption of IMD onto SBA-15 took place. 12% of maximum IMD adsorption onto TiO_2/Cu was observed. No adsorption of IMD onto BP50/P25 took place.

3. Photodegradation of IMD took place with UV irradiation and was analyzed with UV-Vis and HPLC-DAD.

4. HPLC-MS analysis showed at least 5 photoproducts.

5. Reaction rates for IMD degradation were calculated and the evolution of the photoproducts studied. A reaction pathways scheme for the photodegradation of IMD was proposed.

6. It was possible to observe the influence of % of O_2 in the reaction rate of IMD photodegradation.

7. The photocatalytic degradation of IMD in the presence of BP50/P25 under sunlight was observed. The rate constant of the process: $(1,6 \pm 0,2) \cdot 10^{-4}$ s^{-1}.

Conclusións

Durante o desenvolvemento deste proxecto, realicei o estudo da absorbancia UV-Vis do IMD, a fotólise directa UV de IMD, e a fotocatálise heteroxénea de IMD empregando BP50/P25 coma fotocatalizadores. Isto permitiume practicar e mellorar diferentes habilidades, coma:
- traballo autónomo
- traballo en equipo

- planificación de experimentos
- toma de decisions
- análise de resultados experimentais
- emprego de diferentes paquetes de *software* para a análise de datos
- mellora da miña habilidade no uso de diferentes aparellos, coma sistemas de HPLC, espectrofótometros, e fotorreactores
- uso de programas de *plotting* e *fitting* de datos

O traballo tivo unha elevada natureza interdisciplinar, e tiven que usar conceptos e competencias de diferentes asignaturas incluidas no Grao en Química, coma: química orgánica, química analítica instrumental, termodinámica, espectroscopía, química de superficies e cinética.

En conxunto, a miña satisfación con este traballo e o se desenvolvemento é moi elevada.

Os principais descubrimentos deste proxecto foron os seguintes:

1. O coeficiente de absorción molar en pH natural de IMD foi 26671 ± 1304 $M^{-1}\cdot cm^{-1}$ a 270 nm. O espectro non varía co pH.

2. Tivo lugar unha adsorción de IMD en SBA-15 dun 27%. 12% de adsorción máxima de IMD en TiO_2/Cu foi observada. A adsorción de IMD en BP50/P25 non ocorreu.

3. A fotodegradación de IMD tivo lugar con irradiación UV, e foi analizada con UV-Vis e HPLC-DAD.

4. A análise con HPLC-MS demostrou a formación de alomenos 5 fotoprodutos.

5. As constantes de reacción da degradación de IMD foron calculadas e a evolución dos fotoprodutos estudiada. Propúxose un esquema de vías de reación para a fotodegradación de IMD.

6. Observouse a influencia do % de O_2 nas constantes de reacción da fotodegradación de IMD con luz UV.

7. A degradación fotocatalítica de IMD en presencia de BP50/P25 baixo luz solar foi observada. A constante do proceso foi: $(1,6\pm0,2)\cdot10^{-4}$ s^{-1}.

Conclusiones

Durante el desarrollo de este proyecto, realicé el estudio de la absorbancia UV-Vis de IMD, la fotólisis UV directa de IMD, y la fotocatálisis heterogénea de IMD empleando BP50/P25 como fotocatalizadores. Esto me permitió practicar y mejorar diferentes habilidades, como:

- trabajo autónomo
- trabajo en equipo
- planificación de experimentos
- toma de decisiones
- análisis de resultados experimentales
- empleo de diferentes paquetes de *software* para el análisis de datos
- mejora de mi habilidad en el uso de diferentes aparatos, como sistemas de HPLC, espectrofotómetros, y fotorreactores
- uso de programas de *plotting* y *fitting* de datos

El trabajo tuvo una elevada naturaleza interdisciplinar, y tuve que usar conceptos y competencias de diferentes asignaturas incluidas en el Grado en Química, como: química orgánica, química analítica instrumental, termodinámica, espectroscopía, química de superficies y cinética.

En conjunto, mi satisfacción con este trabajo y su desarrollo es muy elevada.

Los hallazgos de este proyecto fueron los siguientes:

1. El coeficiente de absorción molar a pH natural de IMD fue 26671 ± 1304 $M^{-1} \cdot cm^{-1}$ a 270 nm. El espectro no varía con el pH.

2. Tuvo lugar una adsorción de IMD a SBA-15 del 27%. 12% de adsorción máxima de IMD en TiO_2/Cu fue observada. La adsorción de IMD en BP50/P25 no ocurrió.

3. La fotodegradación de IMD tuvo lugar con irradiación UV, y fue analizada con UV-Vis y HPLC-DAD.

4. El análisis con HPLC-MS demostró la formación de al menos 5 fotoproductos.

5. Las constantes de reacción de la degradación de IMD fueron calculadas y la evolución de los fotoproductos estudiada. Se propuso un esquema de vías de

reacción para la fotodegradación de IMD.

6. Se observó la influencia del % de O_2 en las constantes de reacción de la fotodegradación de IMD con luz UV.

7. La degradación fotocatalítica de IMD en presencia de BP59/P25 bajo luz solar fue observada. La constante del proceso fue: $(1,6\pm0,2) \cdot 10^{-4}$ s^{-1}.

Bibliography

[1]. Williams, G. R., Tarpy, D. R., VanEngelsdorp, D., Chauzat, M. P., Cox-Foster, D. L., Delaplane, K. S., Neumann, P., Pettis, J. S., Rogers, R. E. L., & Shutler, D. (2010). *Colony collapse disorder in context*. BioEssays, *32*(10), 845–846. https://doi.org/10.1002/bies.201000075

[2]. European Commission, Food Safety. https://ec.europa.eu/food/animals/live-animals-trade-imports/honey-bees_en (visited on 15-06)

[3]. The Guardian, *EU agrees total ban on bee-harming pesticides,* Damina Carrington. https://www.theguardian.com/environment/2018/apr/27/eu-agrees-total-ban-on-bee-harming-pesticides (visited on 15-06)

[4]. Ihara, M., & Matsuda, K. (2018*).* Neonicotinoids: molecular mechanisms of action, insights into resistance and impact on pollinators. *Current Opinion in Insect Science*, *30*(Ccd), 86–92. https://doi.org/10.1016/j.cois.2018.09.009

[5]. Yamamoto, I.; Casida, J. E. (1999). Nicotinoid Insecticides and the Nicotinic Acetylcholine Receptor, *Springer Japan*. DOI 10.1007/978-4-431-67933-2

[6]. Fossen, M. (2006). Environmental Fate of Imidacloprid. *Regulation*, 1–16.

[7]. Carvalho, R. N., Ceriani, L., & Ippolito, A. (2015). Development of the first Watch List under the Environmental Quality Standards Directive water policy. https://doi.org/10.2788/101376

[8]. Centers for Control Disease and Prevention, EEUU, https://www.cdc.gov/healthywater/drinking/public/water_diseases.html (visited 16-06)

[9]. Water Quality Association, EEUU. https://wqa.org/whats-in-your-water/emerging-contaminants (visited 16-06)

[10]. Zhang, Y., Geißen, S., Gal, C. Carbamazepine and diclofenac: Removal in wastewater treatment plants and occurrence in water bodies, *Chemosphere*, Volume 73, Issue 8, 1151-1161 (2008).

[11]. Centers for Control Disease and Prevention, EEUU, https://www.cdc.gov/healthywater/drinking/public/water_treatment.html (visited

16-06)

[12]. Glaze, W. H., Kang, J. W., & Chapin, D. H. (1987). The chemistry of water treatment processes involving ozone, hydrogen peroxide and ultraviolet radiation. *Ozone: Science & Engineering*, *9*(4), 335–352. https://doi.org/10.1080/01919518708552148

[13]. Deng, Y., & Zhao, R. (2015). Advanced Oxidation Processes (AOPs) in Wastewater Treatment. *Current Pollution Reports*, *1*(3), 167–176. https://doi.org/10.1007/s40726-015-0015-z

[14]. Peyton, G. R., & Fleck, M. J. (1989). *Field-Scale Evaluation of and Preliminary Testing*. *October*.

[15]. Agüera, A., & Fernández-Alba, A. R. (1998). GC-MS and LC-MS evaluation of pesticide degradation products generated through advanced oxidation processes: An overview. *Analusis*, *26*(6), 123–130. https://doi.org/10.1051/analusis:199826060123

[16]. Canle L, M., Fernández, M. I., Martínez, C., & Santaballa, J. A. (2012). (Re)Greening photochemistry: Using light for degrading persistent organic pollutants. *Reviews in Environmental Science and Biotechnology*, *11*(3), 213–221. https://doi.org/10.1007/s11157-012-9275-x

[17]. Wang, X., Ji, R., Zhang, Y., Yang, Y., Fu, C., & Yang, D. (2018). Research on characterization and modeling for ultraviolet degradation of imidacloprid based on absorbance change. *Optik*, *154*, 315–319. https://doi.org/10.1016/j.ijleo.2017.09.110

[18]. Wozniak, B., & Dera, J. (2007). *Atmospheric and Oceanographic Sciences Library*.

[19]. Patent: D. Rodríguez Ramos, Moisés Canle López, Juan Arturo Santaballa López, Silvio David Aguilar Ramírez. Semiconductor-clay composite photocatalyst España, Ecuador, 19/9/2019. Universidade da Coruña, Universidad de Loja (Ecuador)

[20]. Plante, I. (2010). Energetic and chemical reactivity of atomic and molecular oxygen. *NASA Space Radiation Program*, 2–4.

[21]. El-Gendy, N.Sh.; Omran, B.A. (2019). Elvis Fosso-Kankeu (Ed.) Nano and Bio-based Technologies for Wastewater Treatment: Prediction and Control Tools for the Dispersion of Pollutants in the Environment. *Scrivener Publishing LLC*, pp. 205. https://doi.org/10.1002/9781119577119.ch7

[22]. Žabar, R., Komel, T., Fabjan, J., Kralj, M. B., & Trebše, P. (2012). Photocatalytic degradation with immobilised TiO2 of three selected neonicotinoid insecticides: Imidacloprid, thiamethoxam and clothianidin. *Chemosphere*, *89*(3), 293–301. https://doi.org/10.1016/j.chemosphere.2012.04.039

[23]. Wamhoff, H., & Schneider, V. (1999). Photodegradation of imidacloprid. *Journal of Agricultural and Food Chemistry*, *47*(4), 1730–1734. https://doi.org/10.1021/jf980820j

[24]. Agüera, A., & Fernández-Alba, A. R. (1998). GC-MS and LC-MS evaluation of pesticide degradation products generated through advanced oxidation processes: An overview. *Analusis*, *26*(6), 123–130. https://doi.org/10.1051/analusis:199826060123

[25]. Selvarajan, N., Raghavan, N. V. (1980). Reaction of OH with Pyridine. Pulse-radiolytic and Product-Analysis Studies, *Journal of Physical Chemistry, 84(4),* 2548–2551.